AD-A030 882

Evaluation of Parameters Affecting Horizontal Stability of Landing Mats

Army Engineer Waterways Experiment Station Vicksburg Miss

Sep 76

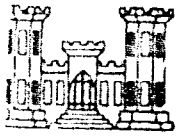

TECHNICAL REPORT S-76-10

EVALUATION OF PARAMETERS AFFECTING HORIZONTAL STABILITY OF LANDING MATS

by

Yu T. Chou, Walter R. Barker, William P. Dawkins

Soils and Pavements Laboratory
U. S. Army Engineer Waterways Experiment Station
P. O. Box 631, Vicksburg, Miss. 39180

September 1976
Final Report

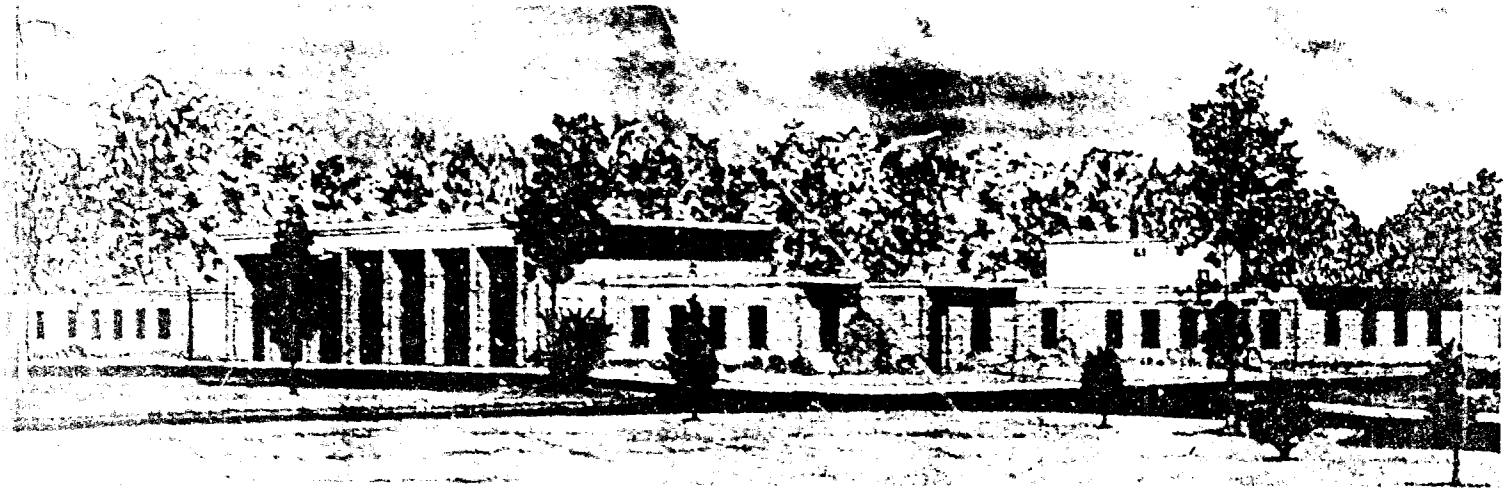

Prepared for Office, Chief of Engineers, U. S. Army
Washington, D. C. 20314

Under Project 4A762719AT31
Task 02, Work Unit 001

Unclassified

SECURITY CLASSIFICATION OF THIS PAGE (When Data Entered)

REPORT DOCUMENTATION PAGE		READ INSTRUCTIONS BEFORE COMPLETING FORM
1. REPORT NUMBER Technical Report S-76-10	2. GOVT ACCESSION NO.	3. RECIPIENT'S CATALOG NUMBER
4. TITLE (and Subtitle) EVALUATION OF PARAMETERS AFFECTING HORIZONTAL STABILITY OF LANDING MATS		5. TYPE OF REPORT & PERIOD COVERED Final report 6. PERFORMING ORG. REPORT NUMBER
7. AUTHOR(s) Yu T. Chou, Walter R. Barker, William P. Dawkins		8. CONTRACT OR GRANT NUMBER(s)
9. PERFORMING ORGANIZATION NAME AND ADDRESS U. S. Army Engineer Waterways Experiment Station Soils and Pavements Laboratory P. O. Box 631, Vicksburg, Mississippi 39180		10. PROGRAM ELEMENT, PROJECT, TASK AREA & WORK UNIT NUMBERS Project 4A762719AT31, Task 02, Work Unit 001
11. CONTROLLING OFFICE NAME AND ADDRESS Office, Chief of Engineers, U. S. Army Washington, D. C. 20314		12. REPORT DATE September 1976 13. NUMBER OF PAGES 67
14. MONITORING AGENCY NAME & ADDRESS(if different from Controlling Office)		15. SECURITY CLASS. (of this report) Unclassified 15a. DECLASSIFICATION/ DOWNGRADING SCHEDULE

16. DISTRIBUTION STATEMENT (of this Report)

Approved for public release; distribution unlimited.

17. DISTRIBUTION STATEMENT (of the abstract entered in Block 20, if different from Report)

18. SUPPLEMENTARY NOTES

19. KEY WORDS (Continue on reverse side if necessary and identify by block number)

Landing mats

20. ABSTRACT (Continue on reverse side if necessary and identify by block number)

The parameters that affect the horizontal stability of airfield surfacing mats were studied by conducting a series of static full-scale buckling tests in the laboratory using various mats and lay patterns. AM2, XM18, and XM19 mats with simulated waterproofing were used in the testing. The mat test sections ranged from one to five panels wide with widths of up to 36 ft. It was found that the most predominant factor affecting the buckling load was the initial eccentricity characteristic of the mat system. Other factors were panel width, mat unit weight, and formation width. The magnitude of locking angle had no effect on the buckling load but did affect the profile of the buckled wave. The existence of resilient filler in the joints of the waterproofing mats reduced the locking angle but did not increase the buckling load.

(Continued)

DD FORM 1 JAN 73 1473 EDITION OF 1 NOV 65 IS OBSOLETE

Unclassified

SECURITY CLASSIFICATION OF THIS PAGE (When Data Entered)

20. ABSTRACT (Continued).

A series of buckling tests of model AM2 mats of various widths were conducted in the laboratory; the mats were obtained from Utah State University. The results enabled the extrapolation of full-scale mat tests from short widths in the laboratory to airfield widths.

Attempts were made to develop a mathematical model to compare with the buckling behavior of the prototype mats. It was found that the horizontal load at which buckling would be initiated depends almost exclusively on the vertical eccentricities existing in the mat at the time the load is applied; because of the random nature of initial irregularities in the real system, the initial buckling load is an unreliable measure of the load-carrying capacity of the system. Therefore, it was concluded that little benefit could be gained from more elaborate mathematical analyses directed toward a more exact determination of initial buckling load or of sustained postbuckling resistance. Analyses were thus made by a simplified articulated system composed of straight rigid bars and movement-free joints. Only qualitative comparisons between the idealized and real systems were made because (a) the joints of the real mat are not movement-free before locking, (b) there are shifts in the joints caused by horizontal load transfer through the joints during buckling.

Methods by which the stability can be increased included several alternative lay patterns. These patterns, which enhance the postbuckling behavior and may increase the initial buckling load, are suggested and explained.

THE CONTENTS OF THIS REPORT ARE NOT TO BE USED FOR ADVERTISING, PUBLICATION, OR PROMOTIONAL PURPOSES. CITATION OF TRADE NAMES DOES NOT CONSTITUTE AN OFFICIAL ENDORSEMENT OR APPROVAL OF THE USE OF SUCH COMMERCIAL PRODUCTS.

PREFACE

The study reported herein was conducted at the U. S. Army Engineer Waterways Experiment Station (WES) under Department of the Army Project 4A762719AT31, Research for Lines of Communication Facilities in Theater of Operations, Military Engineering RDTE Program, Task 02, "Air Line of Communication Facilities," Work Unit 001, "Evaluation of Parameters Affecting the Horizontal Stability of Landing Mats," under the sponsorship and guidance of the Office, Chief of Engineers, U. S. Army.

The study was conducted by Drs. Y. T. Chou and W. R. Barker during the period July 1972-December 1974 under the general supervision of Mr. J. P. Sale, Chief, Soils and Pavements Laboratory. Professor W. P. Dawkins of Oklahoma State University was employed by WES as a technical consultant. This report was prepared by Drs. Chou and Barker. Professor Dawkins prepared Part VI, "Mathematical Analysis of Landing Mats," and made suggestions and comments on the report.

BG E. D. Peixotto, CE, and COL G. H. Hilt, CE, were Directors of WES during the conduct of this investigation and the preparation of this report. Mr. F. R. Brown was the Technical Director.

CONTENTS

CONVERSION FACTORS, U. S. CUSTOMARY TO METRIC (SI) UNITS OF MEASUREMENT

U. S. customary units of measurement used in this report can be converted to metric (SI) units as follows:

Multiply	By	To Obtain
inches	2.54	centimetres
feet	0.3048	metres
square inches	6.4516	square centimetres
pounds (mass)	0.4535924	kilograms
pounds (force)	4.448222	newtons
kips (force)	4.448222	kilonewtons
pounds (force) per square inch	6.894757	kilopascals
pounds (mass) per square foot	4.882428	kilograms per square metre
inch-pounds (force)	0.1129848	newton-metres
foot-pounds (force)	1.355818	newton-metres
inches per minute	2.54	centimetres per minute
knots (international)	0.5144444	metres/second
degrees (angle)	0.01745329	radians

EVALUATION OF PARAMETERS AFFECTING HORIZONTAL STABILITY OF LANDING MATS

PART I: INTRODUCTION

BACKGROUND

1. In August 1970, an experiment on the operations of the C-5A aircraft on the landing mat test facility was conducted at Dyess Air Force Base (AFB), Texas. A failure of an AM2 mat runway system was observed, indicating an instability of mat runways to loads applied by aircraft braking forces during landing operations. A detailed description of the observations of the incident is reported in Reference 1. To facilitate this presentation, the observation is briefly described in the following paragraphs.

2. The landing mat test facility was 6000 ft* long and 96 to 98 ft wide, and consisted of XM18, XM19, and AM2 landing mats. The C-5A used in this operation had an initial gross weight of 480,000 lb with 82-psi tire pressure on the main gears and 108 psi on the nose gear. Prior to the landing which caused the failure incident, the test facility had already experienced four take-offs and three landings. In the fourth landing, the aircraft made an initial main gear touchdown on XM19 mat at a speed of approximately 140 to 150 knots. Only brakes and spoilers were used in stopping the aircraft. The initial damage to the mat originated at the transition between the XM19 and AM2 mats, which is about 1200 ft from the location where braking started. The center portion of the XM19 had shifted in the landing direction approximately 11 in., the underlap-female transition adapter had been bent and distorted, and some of the connector lips were sheared off. The damaged mat was primarily AM2 mat. (XM18 mats were placed in the area behind the AM2 mats.) The damaged AM2 mat had become disconnected along the 12-ft side joints due to joint failure. End joint weld failures were evident with panel distortion of all types. Numerous side joints were torn off and several portions of panels were driven into the ground. Immediately after the incident, a 1.5-ft vertical bow wave existed in some areas and was later rolled out. In the area of incident, the landing mat was underlaid with polypropylene-asphalt waterproofing material with a Herculite membrane cover. The subgrade strength was estimated to be in the range of 10 to 15 California Bearing Ratio (CBR).

3. Several days after the incident at Dyess AFB Lockheed personnel and personnel of various governmental agencies met to review the incident. The main items presented at the meeting were:

   a. The C-5A was braking at 50 percent of maximum with no reverse thrust; however, this could possibly be 100 percent braking at the tires since the antiskid device was cycling.

   b. A 4-in. vertical bow wave had been observed by Lockheed personnel on the AM2 mat on a previous landing after the C-5A stopped on the mat; however, as the aircraft moved forward, the wave disappeared.

   c. High shear forces induced by the [illegible] of the C-5A braking apparently were the general cause of failures in the mat complex.

---

* A table of factors for converting U. S. customary units of measurement to metric (SI) units is presented on page 4.

4. After the failure incident at Dyess AFB, a series of tests and studies were conducted at the U. S. Army Engineer Waterways Experiment Station (WES) and at Utah State University to study the buckling characteristics of landing mats subjected to horizontal loads for better understanding and definition of the problems associated with the C-5A aircraft and landing mat. These studies and tests are briefly described in the following paragraphs.

a. Immediately after the incident, tension and compression tests and tests to determine the coefficient of friction beneath the mat were conducted at WES to obtain additional information concerning the behavior of the AM2 mat. These tests were completed in October 1970. Valuable results were obtained and warranted further full-scale laboratory buckling tests. The material presented in this report is a continuation of the 1970 investigation to further understand the factors affecting the horizontal stability of landing mats. The results of the 1970 study were reported in memorandum form and are included in Appendix A.

b. Following the 1970 tests, extensive skid tests were conducted at WES on XM18, XM19, and T11 landing mats placed in contact with soil and placed on membrane on soil. The results were reported in the form of a memorandum for record.[2]

c. A model study of C-5A landings on AM2 landing mats sponsored by the Air Force Weapons Laboratory (AFWL) was initiated at Utah State University in 1970. A mathematical model to simulate the buckling response of the mats to the horizontal loads was also developed. The results of the study are reported in Reference 3. A meeting was held in 1972 to evaluate Utah State's work and to make recommendations for WES's program to evaluate landing mat behavior under C-5A loadings. The reviewing board consisted of engineers from WES, Professor E. L. Wilson of the University of California, Professor M. E. Harr of Purdue University, and Professor E. J. Barenberg of the University of Illinois. The general consensus of the meeting was that because of the extreme complexity of the problem, it was not practical to attempt an elaborate mechanistic analytical solution; rather, a simpler model dealing with static beam-column-type analysis should be tried. Therefore, Professor W. P. Dawkins of the Oklahoma State University was employed by WES to study and analyze the results of the buckling tests reported herein and to examine the possibility of developing an analytical expression for landing mats subjected to horizontal loads. This report covers the work of Professor Dawkins.

d. At the completion of the model study on AM2 mats, Utah State undertook another series, sponsored by WES, of model studies on heavy-duty truss web mat; theoretical study was not pursued. The results and conclusions of the study are reported in Reference 4. A series of traffic tests and laboratory buckling tests on prototype truss web mats similar to those reported in this study were conducted at WES.

PURPOSE AND SCOPE

5. The purposes of this study were to (a) define and evaluate the parameters that affect the stability of landing mat to horizontal forces, (b) devise methods by which this stability can be increased, and (c) develop an analytical solution to predict the buckling behavior of the landing mat.

6. The primary work involved in this study was an extensive series of laboratory static full-scale buckling tests on AM2, XM18, and XM19 mats and XM18 mats with simulated waterproofing. Mat test sections ranged from one to five panels, the maximum width of a test section was 16 ft. The XM18 mats were tested with simulated waterproofing to determine the effect on buckling loads of the fillers inserted along the joints. A series of buckling tests of model AM2 mat were conducted in the laboratory (the mats were obtained from the Utah State University); the widths of these mat test sections ranged from 0.86 to

13.8 ft. These widths were equivalent to 6 to 96 ft in prototype scale. The purpose of the model testing was to obtain information for extrapolating the laboratory buckling test results to mat sections of greater width. A theoretical analysis was conducted to study the buckling behavior of the mat system, and the results were then compared with experimental data.

PART II: LABORATORY FULL-SCALE BUCKLING TESTS OF LANDING MATS

EQUIPMENT

7. The landing mats were pushed in the lateral direction by a hydraulic loading system (Figure 1). The magnitude of the load and its corresponding lateral movements were recorded electronically and were plotted on a separate X-Y recorder. Load speed was about 6 in./min.

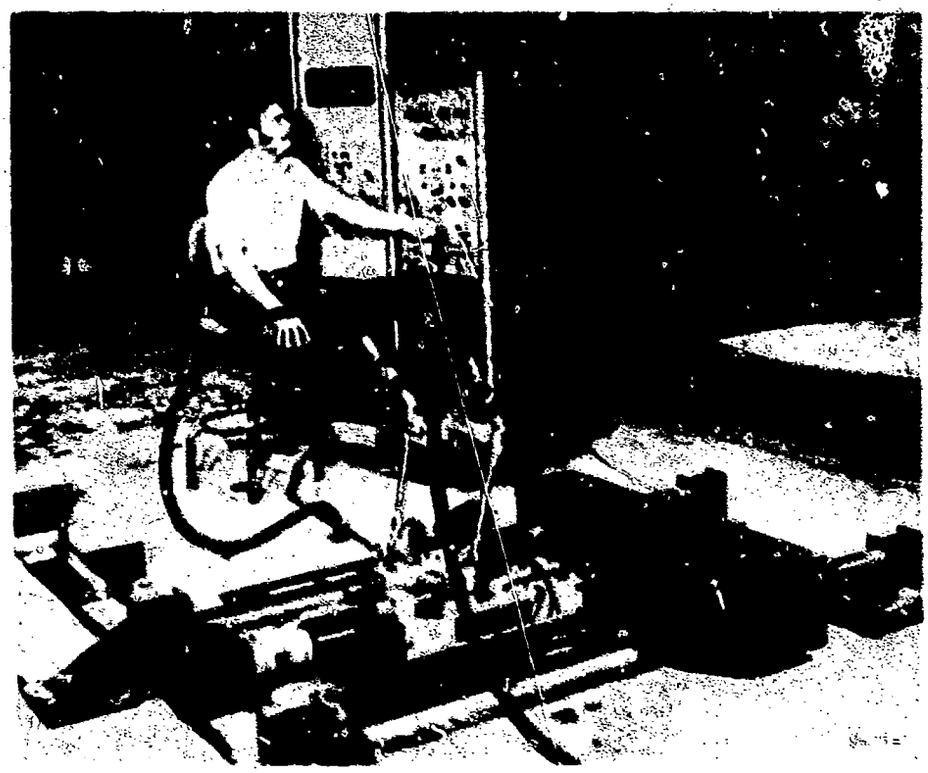

Figure 1. Overall view of the hydraulic loading system

TEST METHOD

8. Twelve runs of mats were generally used in the tests, with the last run bolted to the laboratory's concrete floor. To align the applied forces in the plane of the mat and to reduce the influence of friction forces between the mats and the supporting medium, the mats were placed on steel I beams. Figure 2 is an overall view of a 36-ft-wide mat formation.

9. The width of the mat runway during the C-5A failure incident was 96 ft, and the maximum width of the mat formation tested in the laboratory was 36 ft. Therefore, to simulate the weight of the extra mat, heavy concrete or lead blocks were placed along the two sides of the 36-ft mat system in some tests and the effect on the buckling behavior was studied (Figures 3 and 4). The weight of the lead blocks

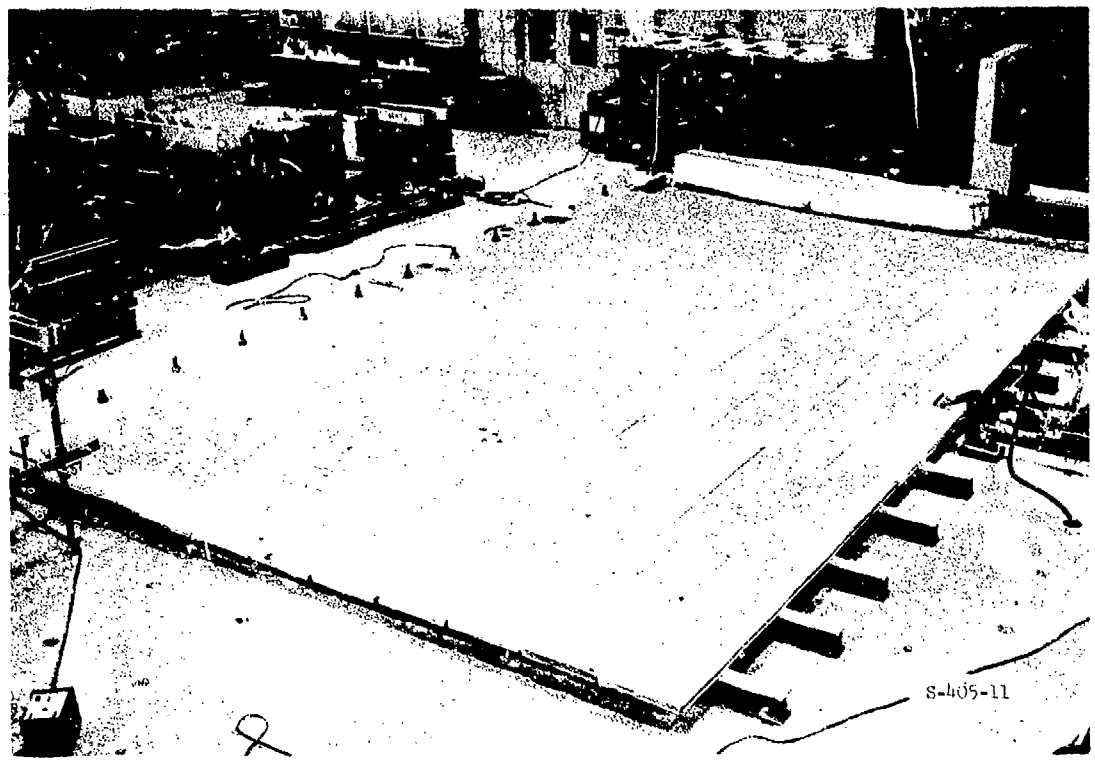

Figure 2. Overview of mat formation

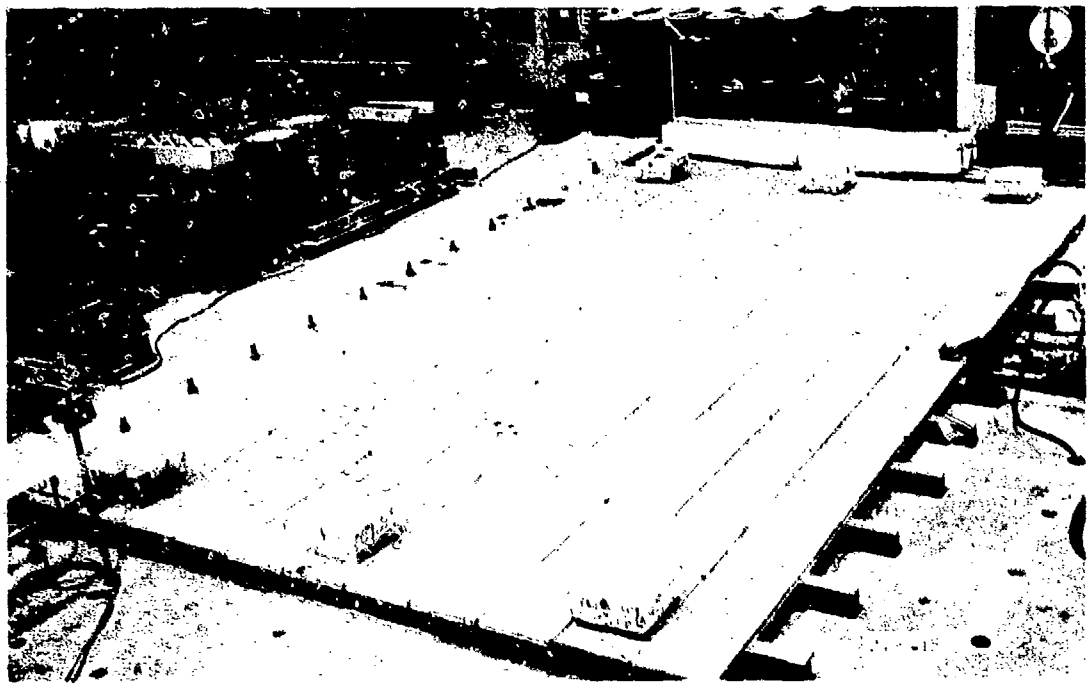

Figure 3. Overall view of mat formation with lead blocks

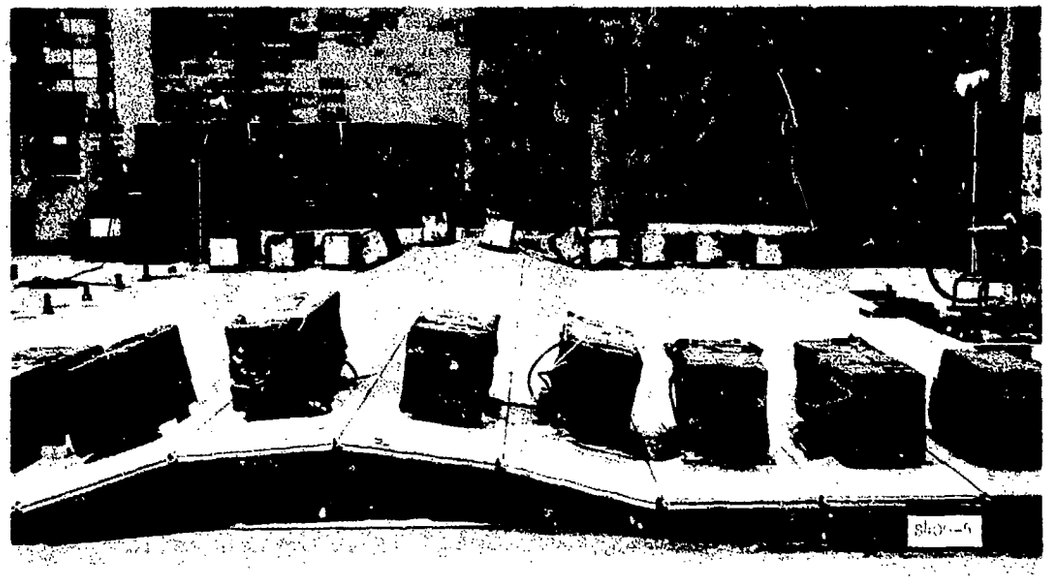

Figure 4. Mat formation with concrete blocks during buckling

was approximately 2000 lb each and that of a concrete block approximately 450 lb; therefore, the concrete block more loosely approximated the weight of the extra width of mat.

10. The shapes of the mat system during the buckling process were measured optically using a level set. The elevations of each mat at the center line of the entire mat system in the longitudinal direction (in the direction of the applied force) were measured before and during the buckling process.

11. Since the mat runways in an actual airfield are never placed on a perfectly flat subgrade surface, eccentricities inevitably exist in the mat system during braking operations. To study the effect of eccentricity on the buckling behavior of the mat, laboratory tests were conducted with a mat system having various magnitudes of eccentricity. Eccentricity was introduced by placing a steel rod across the center line of the mat system in the direction perpendicular to the application of the load.

12. Each mat formation was subjected to repeated buckling tests (generally four or five repetitions). Results of repetitive tests of a formation were found to be reproducible if the mat was pulled to a full extended position after each loading. Otherwise, for a subsequent loading the buckling load was smaller than that of the previous test.

PART III: LABORATORY BUCKLING TESTS OF MODEL AM2 MATS

13. The model AM2 mats were obtained from the Utah State University. The mats were fabricated to a 1/7 scale with respect to the width, length, and weight of the prototype, but were otherwise not in accordance with the engineering similitude law, particularly with respect to the geometry and stiffness of the joints. Figure 5 shows two model mats connected along the side joint. A detailed description of the mats can be found in Reference 3.

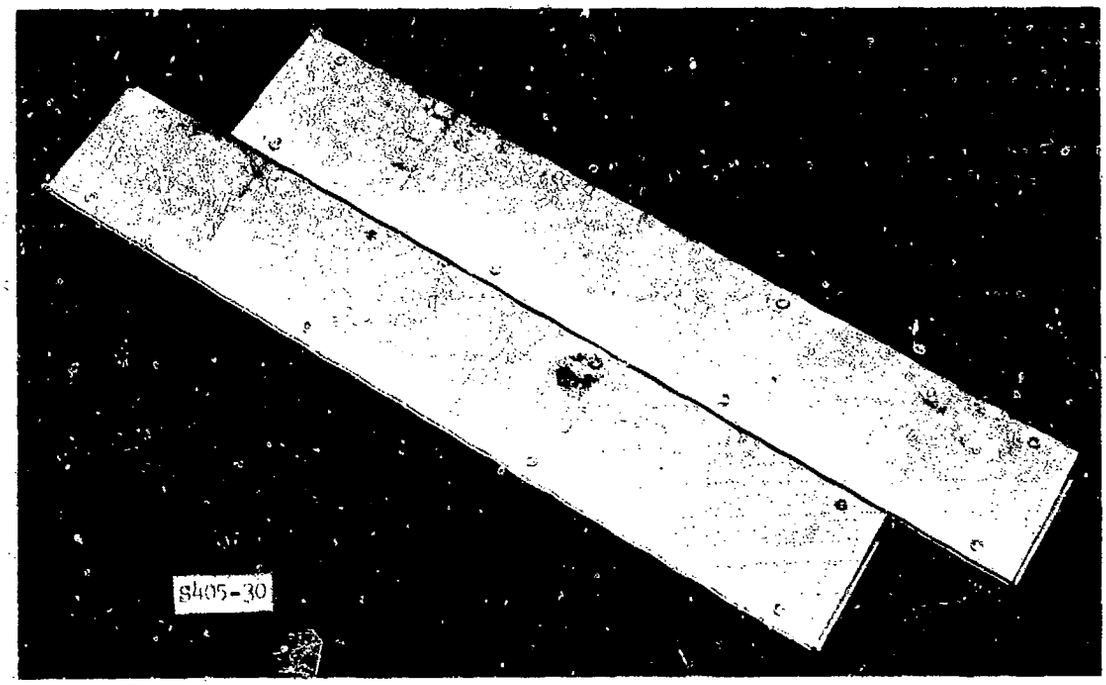

Figure 5. Model AM2 mat

14. Tests were conducted on various widths ranging from one to eight panels. The width of the eight-panel formation corresponds to the 96-ft width of the prototype mat runway at Dyess AFB. Figure 6 shows the setup of the model buckling test; the load was applied to the mat by a field CBR machine through an arrangement to simulate the horizontal force applied by two C-5A 12-wheel gear assemblies. Tests were also conducted by pushing the mats with the CBR piston, which has a diameter of 2 in.

15. Because the joints of the model mats were very weak, difficulty was experienced in assembling the mats. In some cases, the mats had to be pried open by a knife for assembly purposes. Unlike the prototype buckling tests, reproducible results could not be obtained in the model mat testing the buckling load always decreased as the test was repeated. Evidently, the joints were bent once the mats were buckled; the subsequent buckling load decreased because of the damaged joints even though the mats were returned to a fully extended position before the test was repeated.

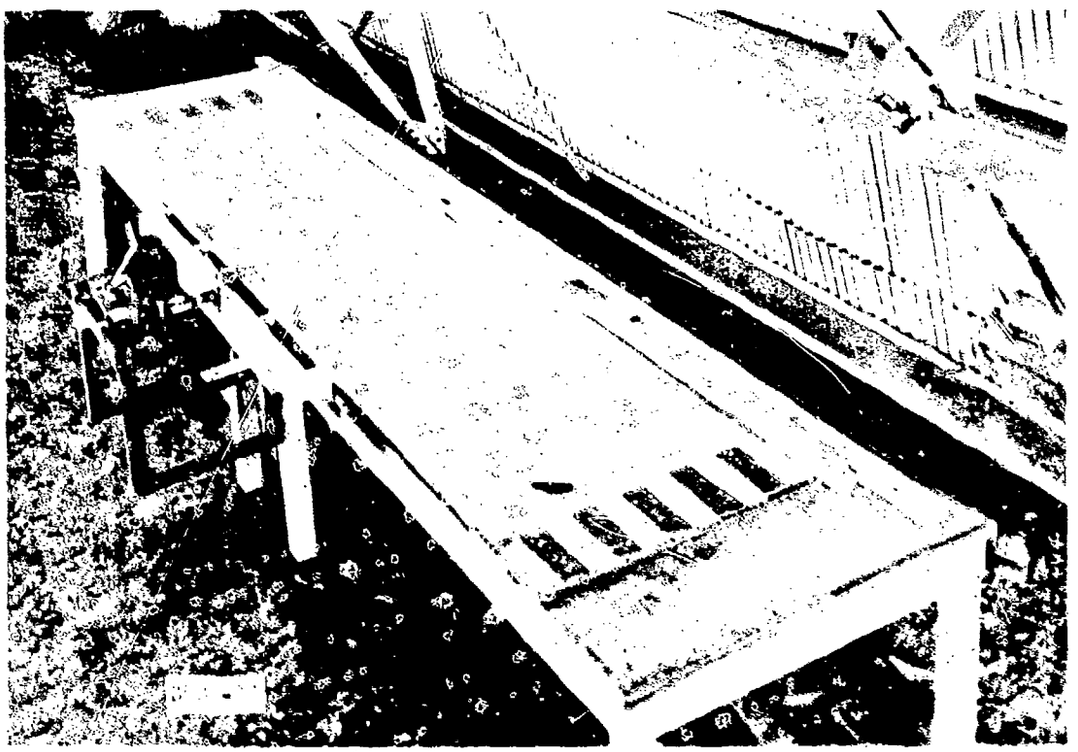

Figure 8. Setup of model AM2 buckling tests

PART IV: ANALYSIS AND PRESENTATION OF RESULTS

CHARACTERISTICS OF MATS TESTED

16. General descriptions of AM2, XM18, and XM19 mats can be found in References 5, 6, and 7, respectively, and are not repeated in this report. Waterproof XM18 mats were not available during the tests; however, tests were conducted on XM18 mats with a heavy-duty rubber hose and plastic wires inserted along the joints. It is believed that the mats with the inserts simulated prototype waterproof mats insofar as buckling tests are concerned.

MODEL AM2 MATS

17. Figure 7 shows the relationships between mat width and buckling load for model AM2 mats. Curve A shows the results for the mats pushed by the 3-sq-in. CBR piston. It can be seen that the buckling load increased almost linearly with increasing mat width; as the number of mats increased beyond three panels (or 36 ft in prototype) the buckling load rate of increase began to slow. As the number of the mats was increased beyond five panels (or 60 ft in prototype), the rate of increase dropped sharply. Curve B shows the results for the mats pushed by the two simulated C-5A 12-wheel gear assemblies.

18. As explained earlier, the purpose of the laboratory tests was to obtain information to extrapolate laboratory results of buckling tests to mat formation of greater width. Figure 7 provides this information. It should be noted, however, that since the model mats were not manufactured according to engineering similitude laws and the joints were very weak, the information provided in Figure 7 should be viewed as a crude approximation.

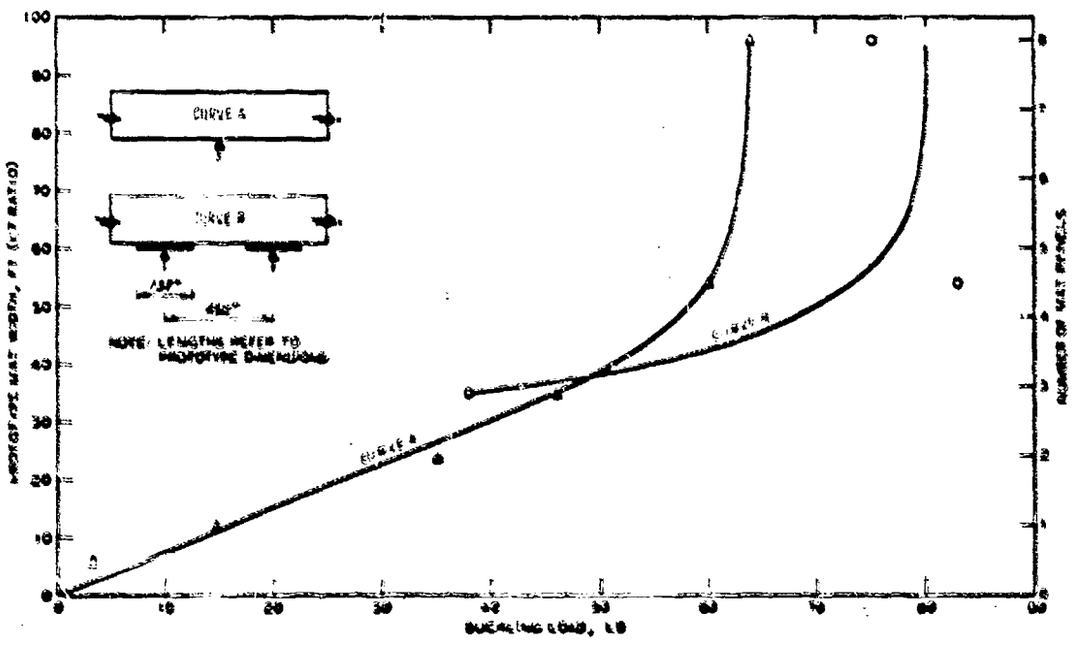

Figure 7. Relationships between mat width and buckling load for model AM2 mats

PROTOTYPE BUCKLING TESTS

19. The joint configurations at both sides of the mat in compressed and buckled up positions for XM19, AM2, and XM18 mats are shown in Figure 8. The contact points between two pieces of mat are shown in the figures. The dimensions are very similar between AM2 and XM18 mats; therefore, some dimensions of the two mats are presented. It should be noted that the dimensions of landing mats vary from one to the other; the information presented in Figure 8 is measured from the specific mats. For instance, the contact points may be more than those shown in Figure 8 as the buckling process continues.

XM19 Mats

20. The honeycomb XM19 mat is a 4- by 4-ft square mat with a unit weight of 4.1 psf. The tests were conducted with mat formation widths of one, three, and five panels, and with the connector bars perpendicular and parallel to the load application. The tests were also performed with the square mats staggered with the connector bars in the position perpendicular to the load, which is the normal method of placement.

21. The locking angle of the longitudinal joint (which is parallel to the landing direction in the actual laying pattern) is larger than that of the transverse joint (which is perpendicular to the landing direction and has the connector bar); the locking angles are approximately 10 and 4 deg, respectively. However, these angles vary greatly with different mats. The locking angle is defined as the maximum angle at the joint between two adjacent panels at which free rotation can exist. Tables 1 and 2 show the results of buckling tests of the XM19 mats with the connector bars perpendicular and parallel to the load, respectively. The mat formation had a width of 20 ft (five panels). The vertical movement values at each of the 12 panels delineate the shapes of the buckled mats at different horizontal movements; they are shown in Figures 9 and 10, respectively, corresponding to Tables 1 and 2. It is seen that although the maximum buckling loads were nearly the same, the shapes of the buckled mats were distinctly different. When the joint with connector bars (transverse joint) is perpendicular to the load, the shape of the mats under the buckling load was similar to a continuous plate, because the locking angle along the transverse joint is small (about 4 deg); the maximum buckling load was obtained during the first buckling and the loads decreased as the height of the buckled mat continued to increase. It is believed that more panels would be buckled and the height of the buckled mats would continue to increase if the length of the mat system had been increased during the test.

22. Because the locking angle along the longitudinal joint (joints without connector pins) is large (about 10 deg) fewer panels were displaced vertically during buckling than when the transverse joints were perpendicular to the load. It is believed that if the buckling process was continued, the mat would break along the joints at locations 8 and 9 in Figure 10.

23. At the top of Figure 11, the shapes of the buckled mats at locations 7-10 of Figure 10 during the last two consecutive loading stages are presented. The figures were drawn to the same scale in both vertical and horizontal directions. It is seen that the angle at location 9 was 15 deg at the end of the test, which was 5 deg greater than the locking angle of the joints. It should be pointed out that at locations 7 and 10 the mat could rotate freely. In the middle of Figure 11, the shapes of the buckled mats of Figure 9 are presented. The angles at locations 8 and 9 were 8 deg, which was much larger than the 4-deg measured locking angle. As noted earlier the measured locking angle varies greatly with different mats; the measured 4-deg angle may be less than the true average value.

24. In this study, it was hypothesized that the buckling load would increase if the locking angle of

COMPRESSED POSITION

INITIAL BUCKLED POSITION

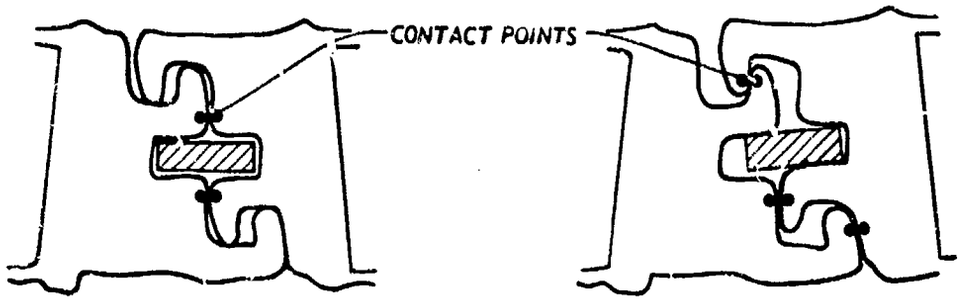

TRANSVERSE JOINT PERPENDICULAR TO LANDING

LONGITUDINAL JOINT PARALLEL TO LANDING

XM19

COMPRESSED POSITION

BUCKLED POSITION

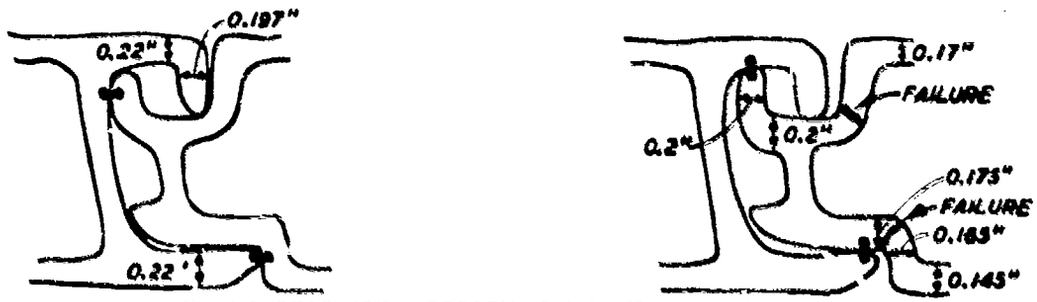

TRANSVERSE JOINT PERPENDICULAR TO LANDING

AM2

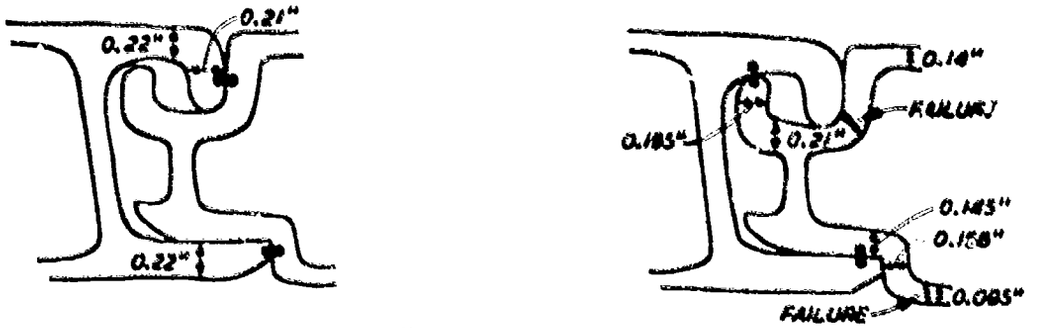

TRANSVERSE JOINT PERPENDICULAR TO LANDING

Figure 8 Configurations of joints in compressed and buckled positions

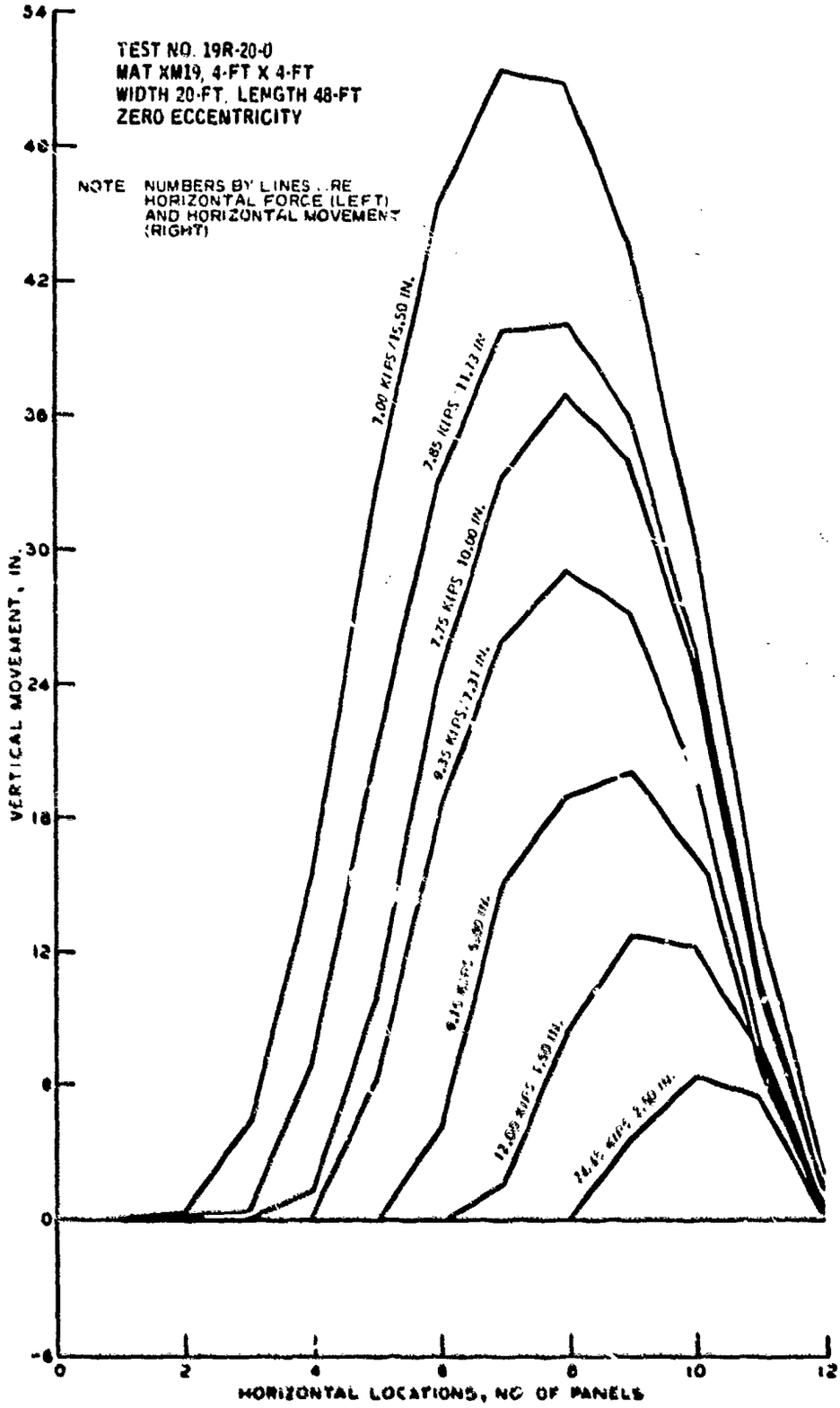

Figure 9. Shapes of buckled XM19 square mats with connector pins perpendicular to the load, mats not staggered

the joint could be reduced. The results shown in Figures 9-11 indicate that the locking angle affects the shape of the buckled mat surface but not the buckling load. The influence of the locking angle will be discussed subsequently. Although the maximum buckling loads are nearly the same, the advantage of having a continuous and smooth buckled mat surface as shown in Figure 9 may be rewarding; the bow wave appeared to be so flexible that the chance for the mat to break is believed to be smaller than when the mats have an abrupt surface as shown in Figure 10.

25. Table 3 shows the test results of staggered XM19 square mats with connector bars

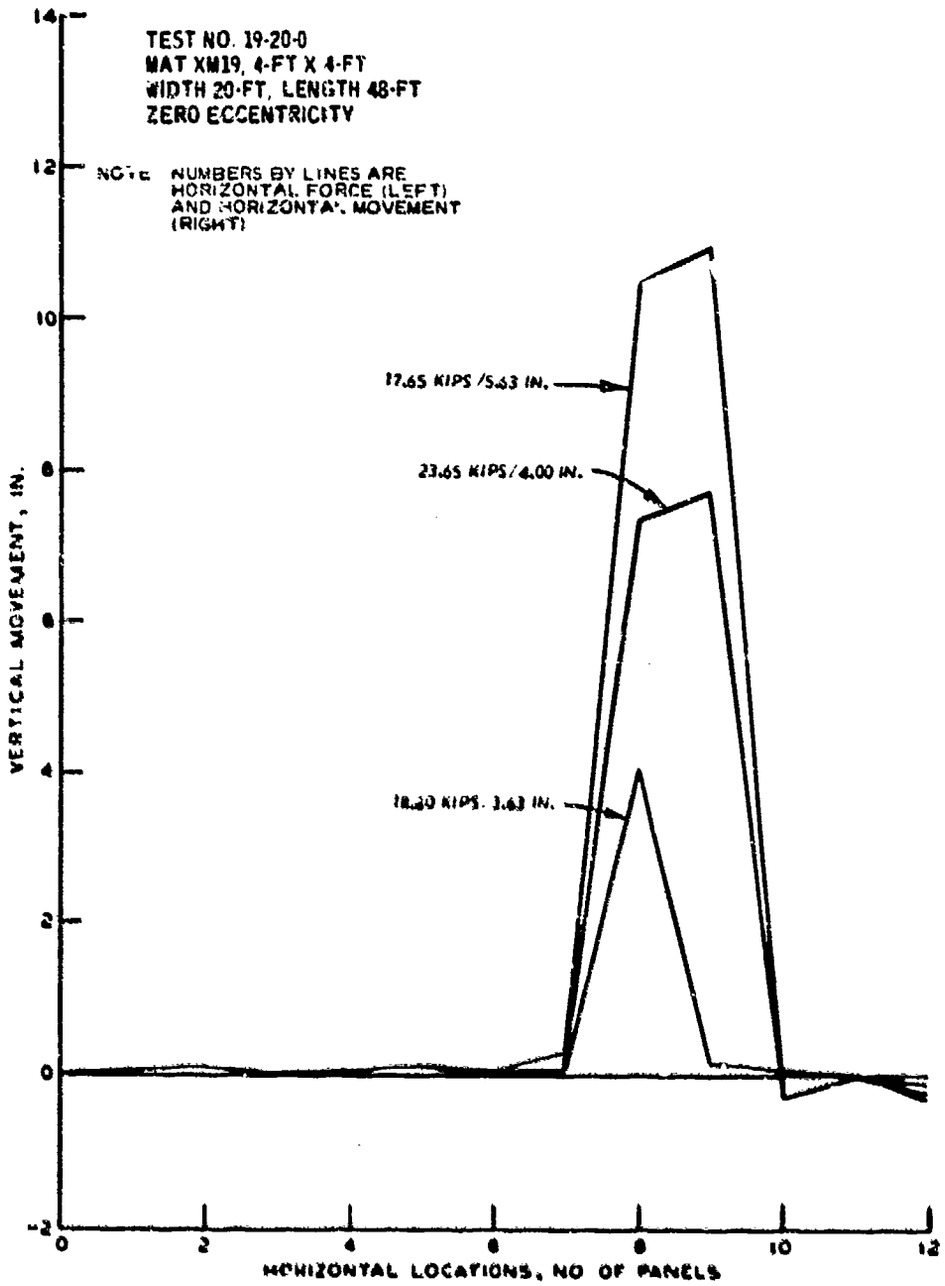

Figure 10. Shapes of buckled XM19 square mats with connector pins parallel to the load, mats staggered

perpendicular to the load. The maximum buckling load was nearly doubled as compared with the mat system when joints perpendicular to the load were not staggered (Figure 9 and Table 1). Figure 12 shows the shapes of the buckled mats at three consecutive loading stages. It can be noted that when compared, at the same horizontal movement, the heights of the buckled mats were about the same whether the mats were staggered (Figure 12) or not (Figure 9). The shapes of the staggered mats during the two last loading stages are shown at the bottom of Figure 11.

26. Figure 13 shows the effects of eccentricity on the maximum buckling loads of XM19 mats. The maximum eccentricity used in the tests was 1 in. It is seen that for mat formations of one-mat width, i.e., 4 ft, and 12 ft with joints not staggered, eccentricity did not affect the buckling loads. The test results were rather inconsistent for mats with staggered joints. This may be due to the fact that the mats were not laid exactly flat at the zero-eccentricity position, i.e., the mats had initial eccentricities in some areas because of roughness and irregularity in the joints. Consequently when the 0.5-in. eccentricity was induced, the mat system became flatter and the buckling loads were thus increased. In most cases, the buckling loads were greatly decreased when the eccentricity was increased to 1 in.

AM2 Mats

27. The aluminum AM2 landing mat is 12 ft long and 2 ft wide with a unit weight of 6.1 psf. Tests were conducted with widths of 6, 12, and 24 ft, and were conducted only with the connector bars parallel to the load application which is the actual laying pattern in airfield runways. The measured locking angle of the AM2 mat is about 10 deg.

28. Table 4 shows the test results of AM2 mat complex with a width of 24 ft. Figure 14 depicts the shapes of buckled mats. Because the locking angle is relatively large, the surface of buckled AM2 mat was not so smooth and continuous as that of the XM19 mat with connector pins perpendicular to the load (see Figure 9); however, it was smoother than that of the XM19 mat with connector pins parallel to the load (see Figure 10).

29. Figure 15 shows the effects of eccentricity on buckling loads of AM2 mats. In the tests with 6-ft-wide half panel, a concrete block was placed near the load application to prevent the premature buckling of the mat at that panel. Figure 15 indicates that the buckling loads were very sensitive to eccentricity.

XM18 Mats

30. The aluminum XM18 mat is geometrically similar to AM2 mat, i.e., 12 ft long and 2 ft wide. The unit weight of XM18 mat is 4.7 psf, which is substantially less than that of the AM2 mat (6.1 psf). The locking angle of the XM18 mat is approximately the same as that of the AM2 mat (about 10 deg). Tests were conducted with widths of 6, 12, 24, and 36 ft, and with the connector bars only parallel to the direction of the applied load, which is the actual laying pattern in airfield runways. Table 5 shows the test results of 24-ft-wide XM18 mats. In Figure 16, the shapes of buckled XM18 mats are illustrated.

31. The effects of eccentricity and mat width on buckling loads of XM18 mats are shown in Figure 17. As in the tests of other mats, the buckling loads decrease with increased eccentricity. Also, the buckling loads increase with increasing width of the mats at all three eccentricities.

32. Because the maximum width of mat system tested in the laboratory was 36 ft and the mat runway used in the Dyess AFB had a width of 96 ft, concrete blocks were placed along the edges of the 36-ft mat system to simulate the added weight of the additional width of mat. Test results with and without the blocks are shown in Figure 18 for induced eccentricities of 0, 0.5, and 1 in. As was expected, the buckling loads increased with the addition of blocks, although induced eccentricity appears to have

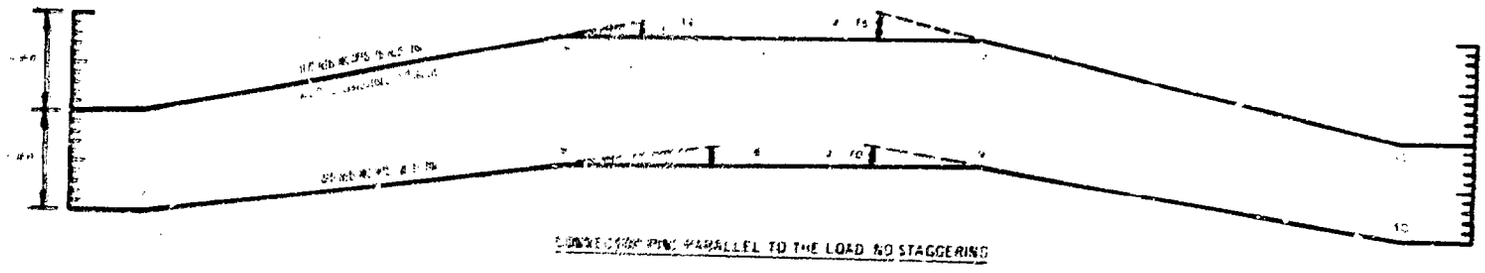

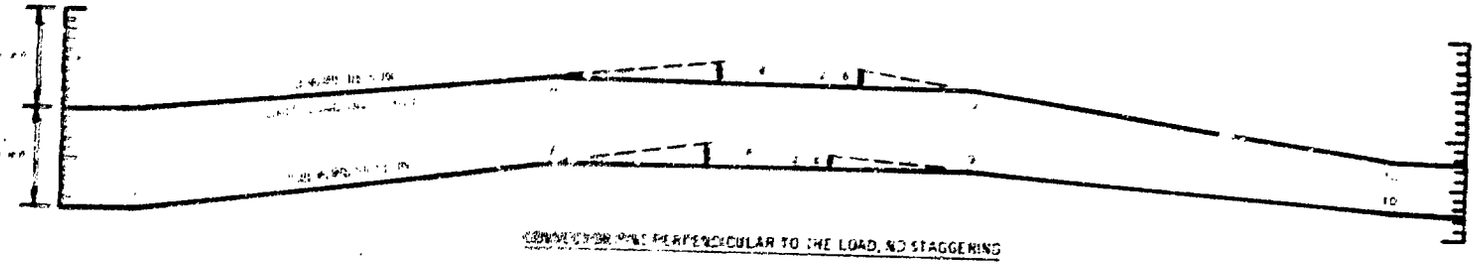

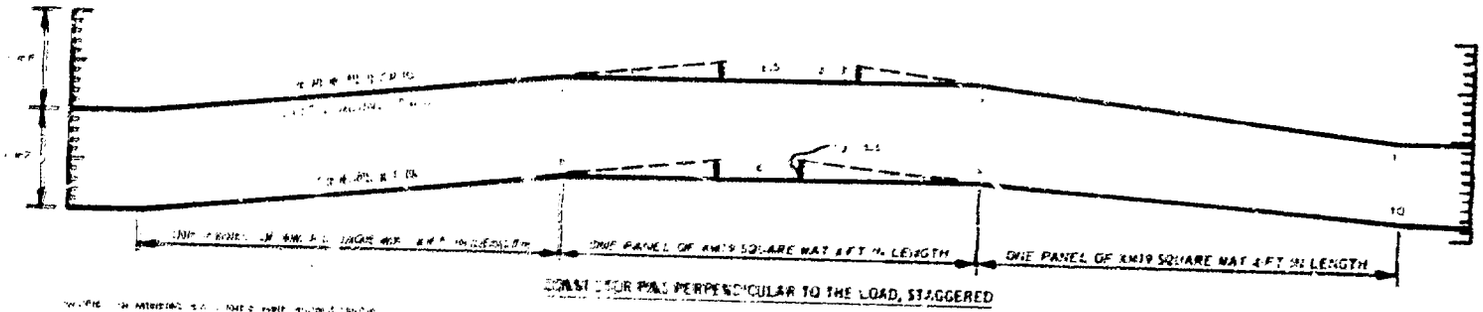

Figure 11 Shapes of buckled XM19 square mats, same scale in vertical and horizontal directions

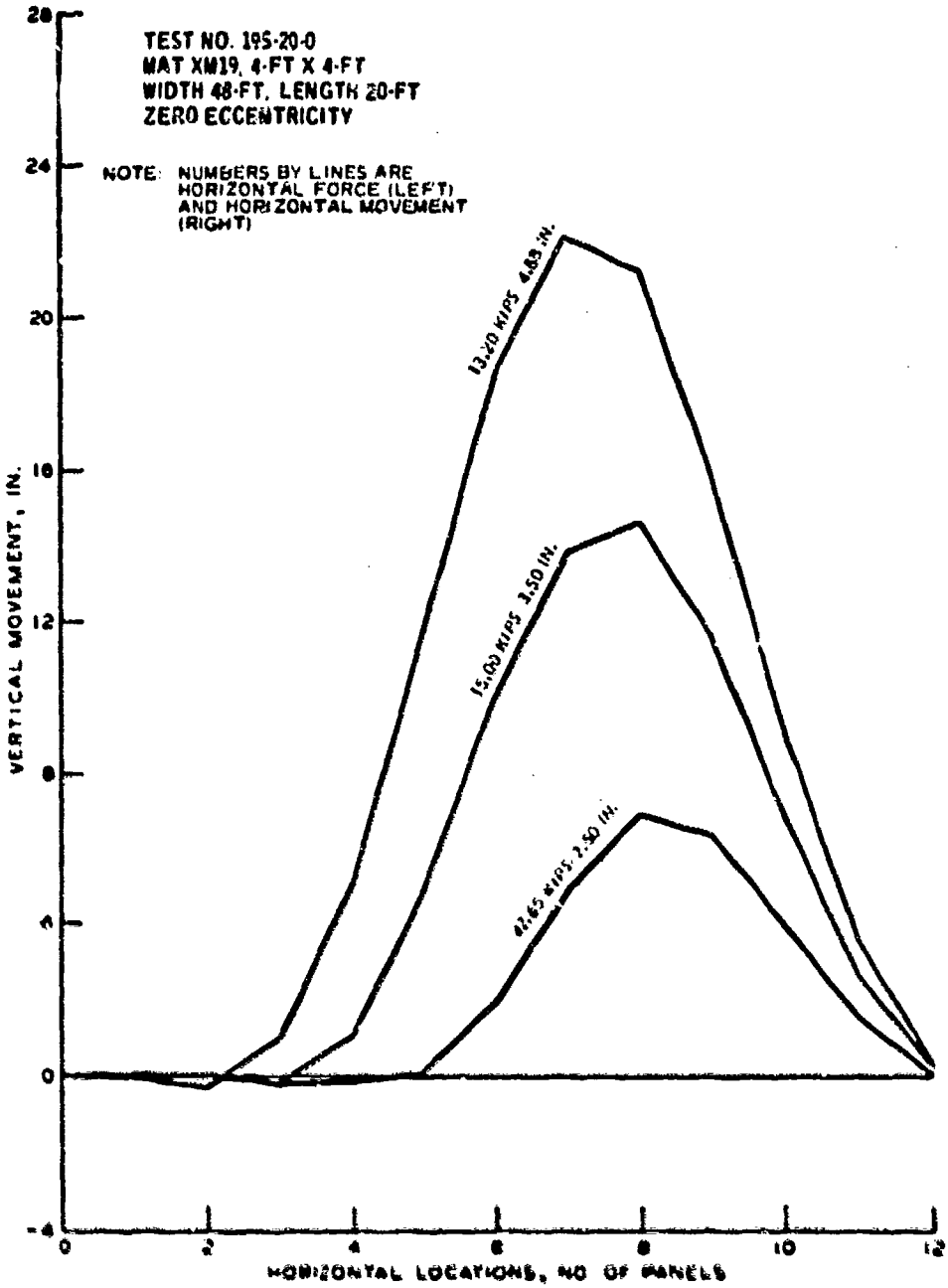

Figure 17. Shapes of buckled XM19 square mats with connector pins perpendicular to the load, mats staggered

little effect. The results of the model AM2 mats shown in Par. III may be used to obtain qualitative information for increased buckling loads due to increasing width of the mats beyond the 36-ft width.

33. The aircraft does not always land at the center of the runway, so tests were conducted with the load applied near the edge of the mat system. The results are shown in Figure 18. It can be seen that the buckling loads were greatly reduced when the loads were not applied at the center of the mats.

34. Figures 19-21 show the surfaces of several buckled XM18 mat systems with and without

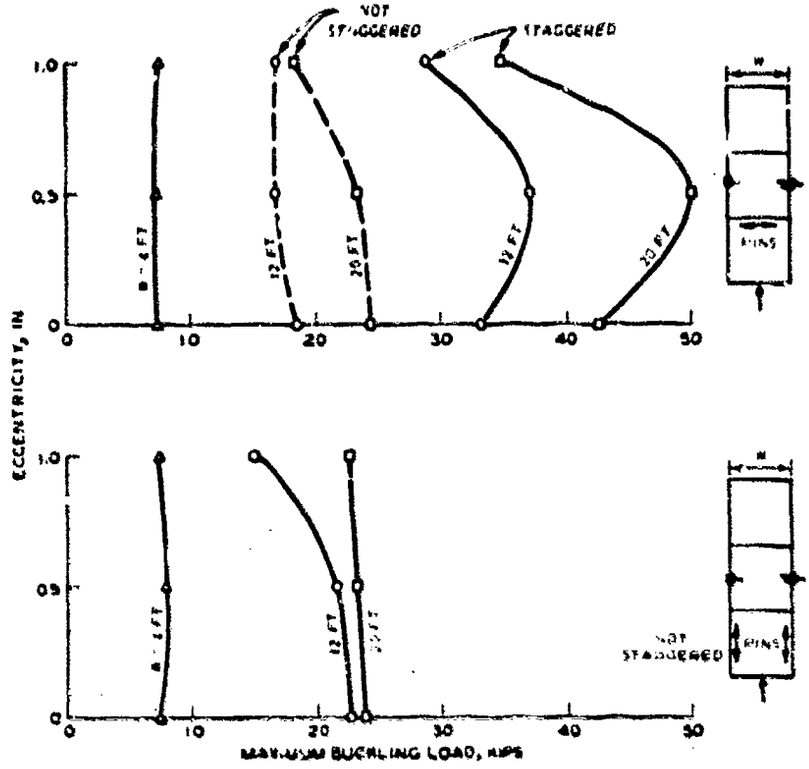

Figure 13. Effects of eccentricity on buckling loads of XM19 mats

concrete blocks. Figure 22 shows the buckled surface when failure of the joints was incipient. Figure 23 shows closeup views of failed joints. For other tests conducted in this study, the buckling process was discontinued long before failure became incipient.

COMPARISON OF BUCKLING LOADS OF DIFFERENT MATS

35. The relationships between buckling loads and mat width for different mats are shown in Figure 24. Except for XM19 mats when the joints were not staggered, the buckling loads of the mats increased linearly with increasing mat width within the range of tests. The maximum buckling load was obtained with staggered XM19 mats in which the connector bars were perpendicular to the load. When the XM19 mats were not staggered, the tests were conducted with connector bars both perpendicular and parallel to the loads. The buckling loads for this case were larger than for AM2 mats at 12-ft width but smaller than for AM2 mats at 20-ft width. The reason for the nonlinear relationship between buckling loads and mat width for the XM19 mats is not known. Because the unit weight of XM19 is close to that of XM18 mat, the greater buckling load of XM19 (with mats not staggered) compared with that of the XM18 mat is attributable to the greater panel width of the XM19 mats (i.e., greater distance between panel joints in the direction of loading).

36. The unit weight of the XM19 mat is substantially less than that of AM2 mats. However, the buckling load of the XM19 mats in a staggered laying pattern is much greater than the buckling load of the AM2 mat. As can be seen in Figure 24, staggering the joints of the XM19 mat greatly increased the

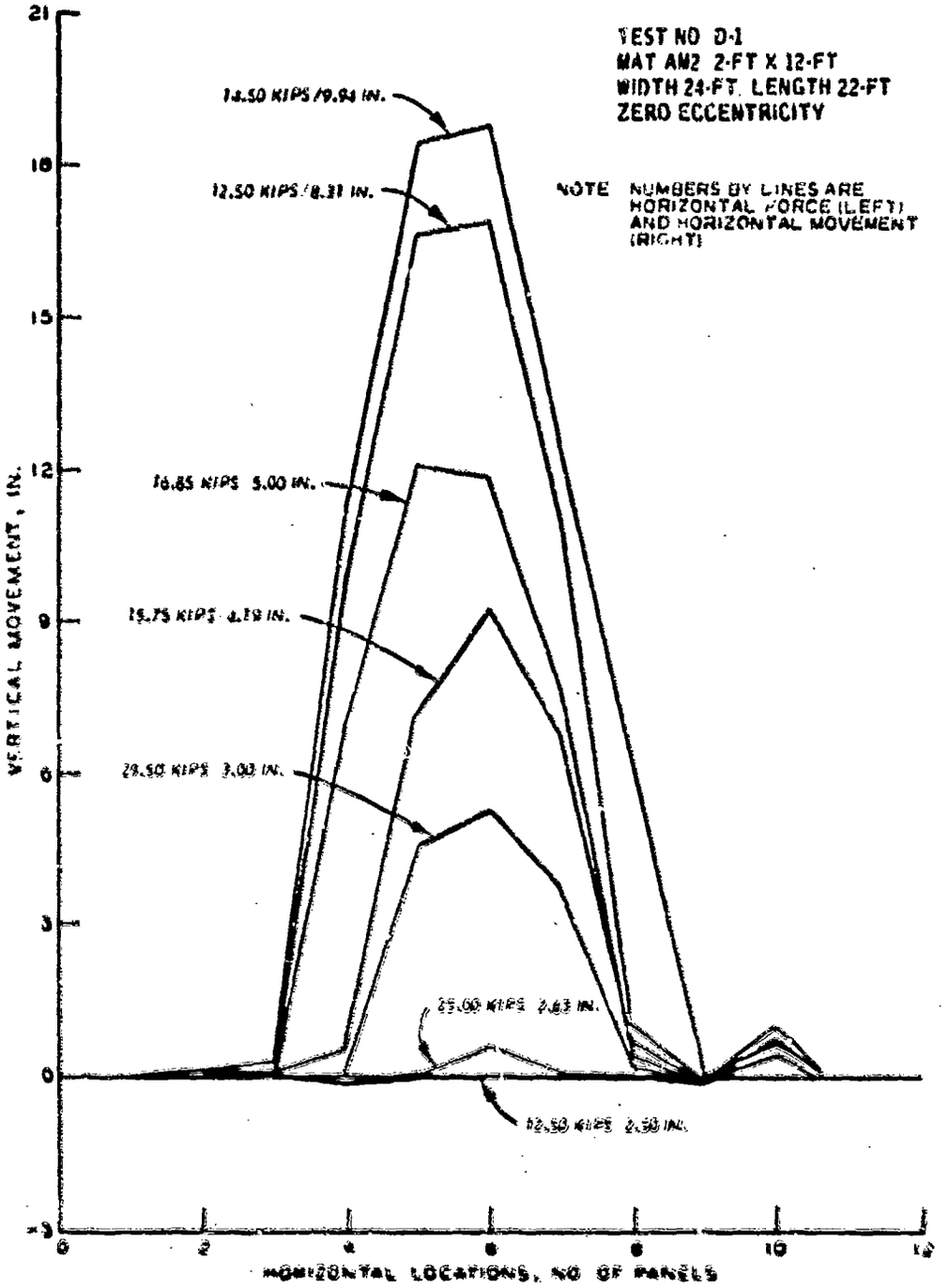

Figure 14. Shapes of buckled AM2 mats, 24 ft wide

buckling load. In the staggered lay pattern, behavior of the XM19 mat approaches that of a continuous plate, which in theory would offer the maximum possible resistance to buckling, if the weight and other characteristics of the mat remain constant. Thus the test results from the XM19 in a staggered lay pattern represent the maximum resistance to buckling that can be reasonably expected from this or similar mats.

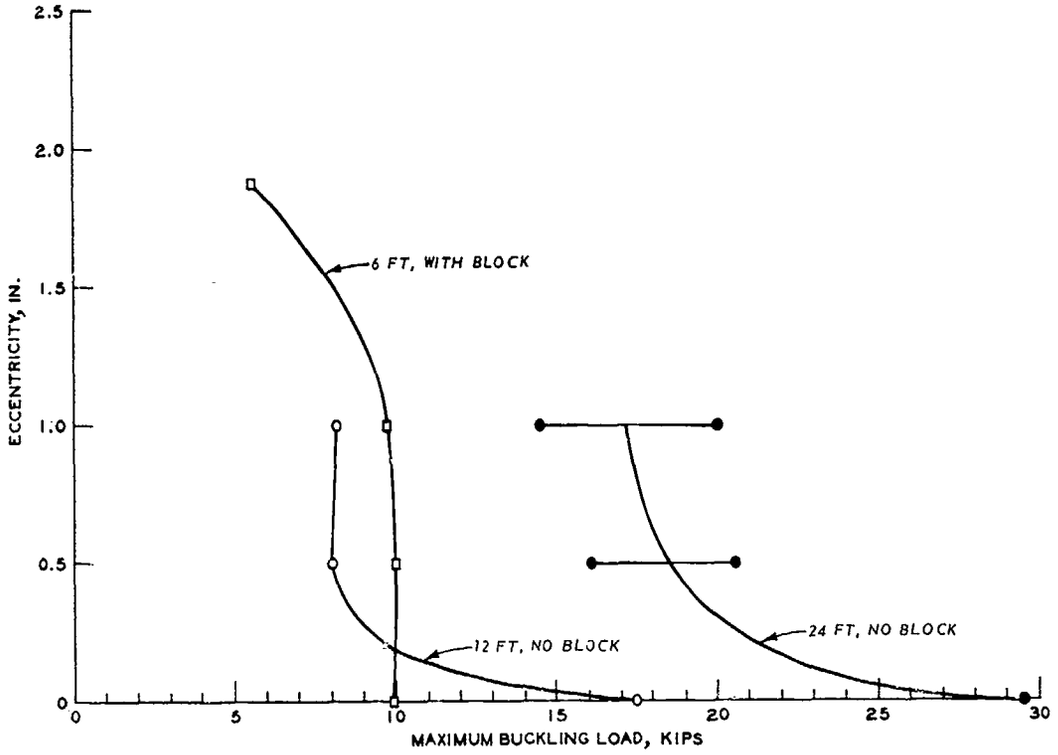

Figure 15. Effects of eccentricity on buckling loads of AM2 mats

37. The joints of AM2 and XM18 mats are very similar, as shown in Figure 8. However, the dimensions shown in the figure may vary greatly among different mat sections.

SIMULATED WATERPROOF XM18 MATS

38. The purpose of the tests of simulated waterproof mats was to determine the effect of the fillers inserted along the joints on the buckling loads. Prior to the tests, it was considered that the filler insertion would reduce the locking angle and thus increase the buckling loads. As previously mentioned, waterproof XM18 mats were not available during the tests; thus a 0.5-in. (outside diameter) heavy-duty rubber hose was used as shown in Figure 25. Because of difficulty in inserting the hose along the full length of the transverse joint, 6-in. pieces of hose were placed at two sides and the center of each panel. It is believed that this arrangement was an adequate simulation of the waterproof XM18 mats. Tests were also performed with a 5/16-in.-diameter, plastic-coated utility wire inserted along the joint as also shown in Figure 25.

39. Test results for a 6-ft-wide mat showed no increase of buckling load with the insertions along the joint. Tests were also conducted with the center of the rubber hose filled with plastic wire to increase its stiffness, but no increase of buckling load was observed. However, it was found that the surface of the buckled mat with insertions was much smoother and more continuous than that of the buckled mats without insertions. This is particularly true when plastic-coated wires were placed at the upper part of the joint. Tests with mat width greater than 6 ft were not conducted.

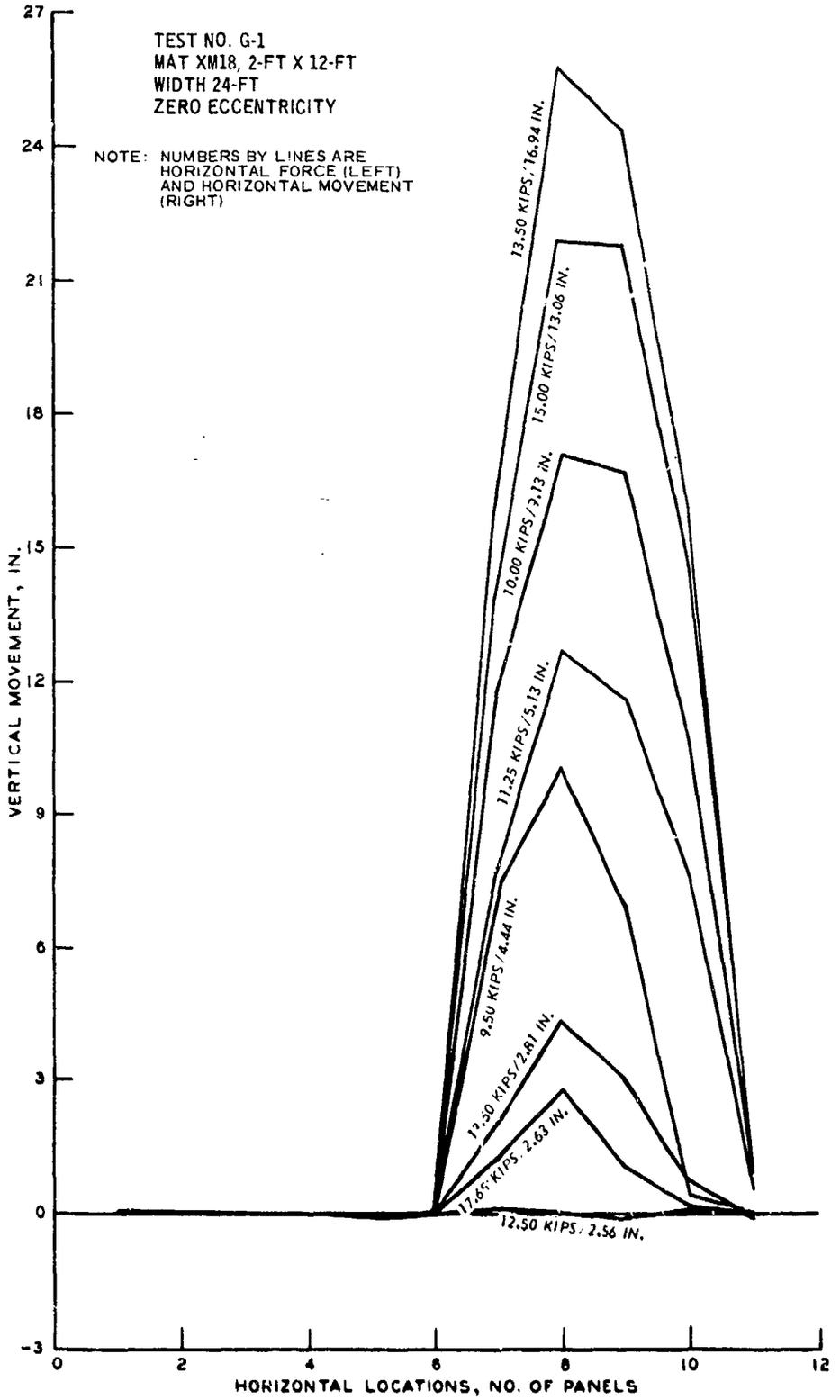

Figure 16. Shapes of buckled XM18 mats, 24 ft wide

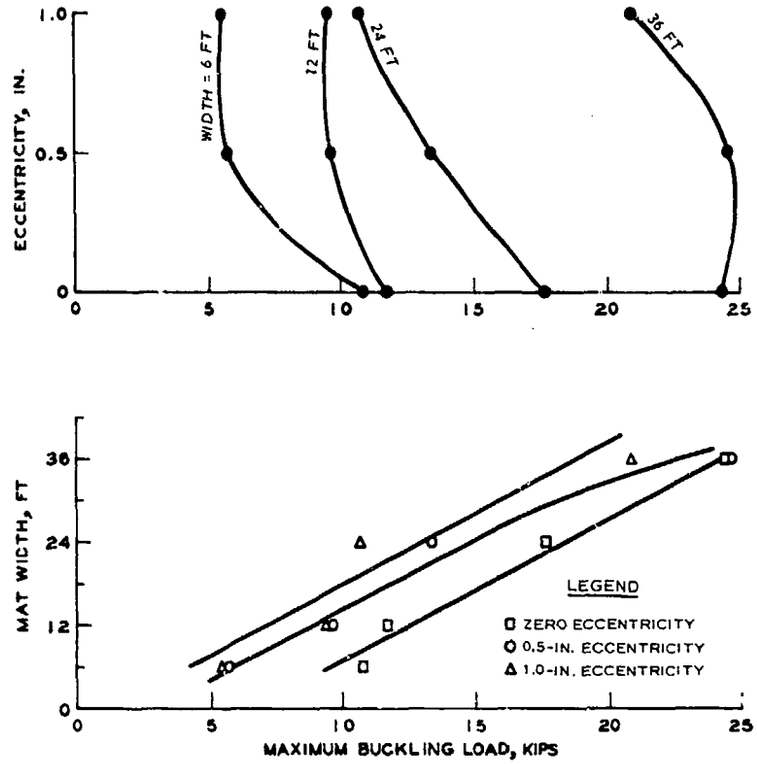

Figure 17. Effects of eccentricity and mat width on buckling loads of XM18 mats

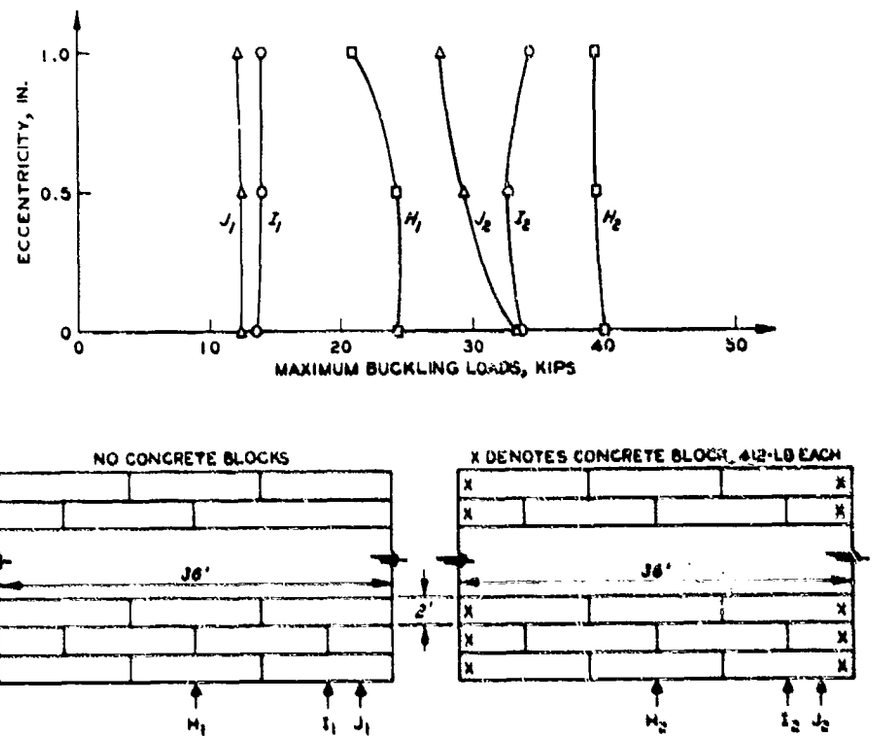

Figure 18. Effects of side constraints on buckling loads at differing eccentricity, XM18 mats

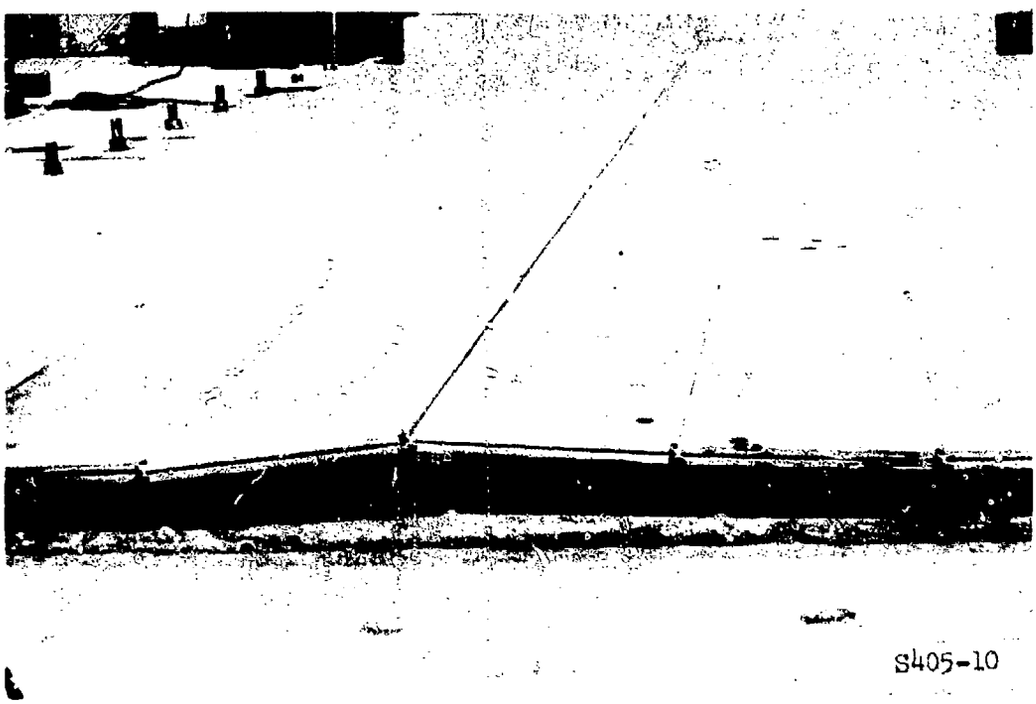

Figure 19. Surface of 36-ft-wide XM18 mats after first buckling

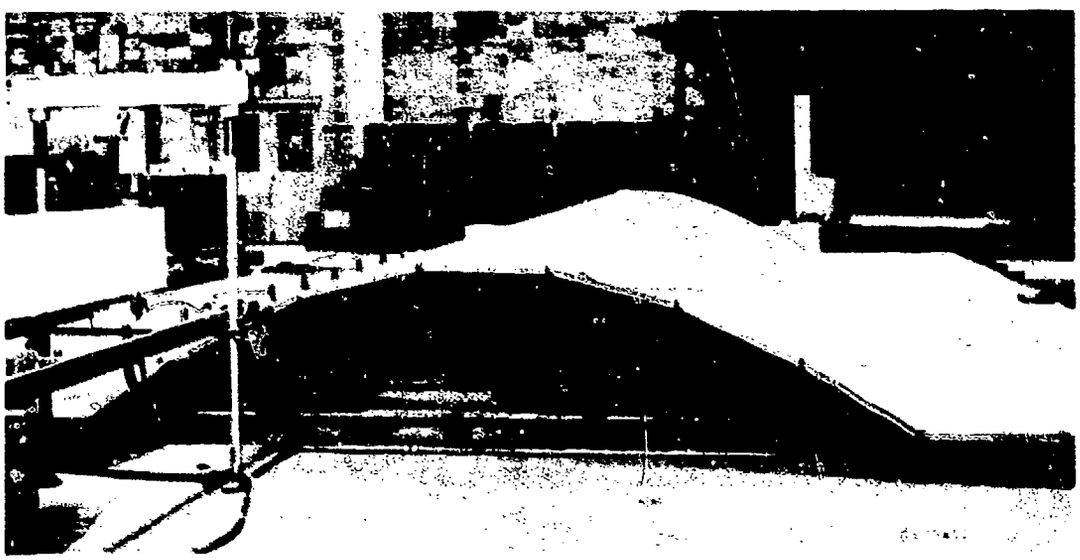

Figure 20 Buckled surface of XM18 mats 36 ft wide

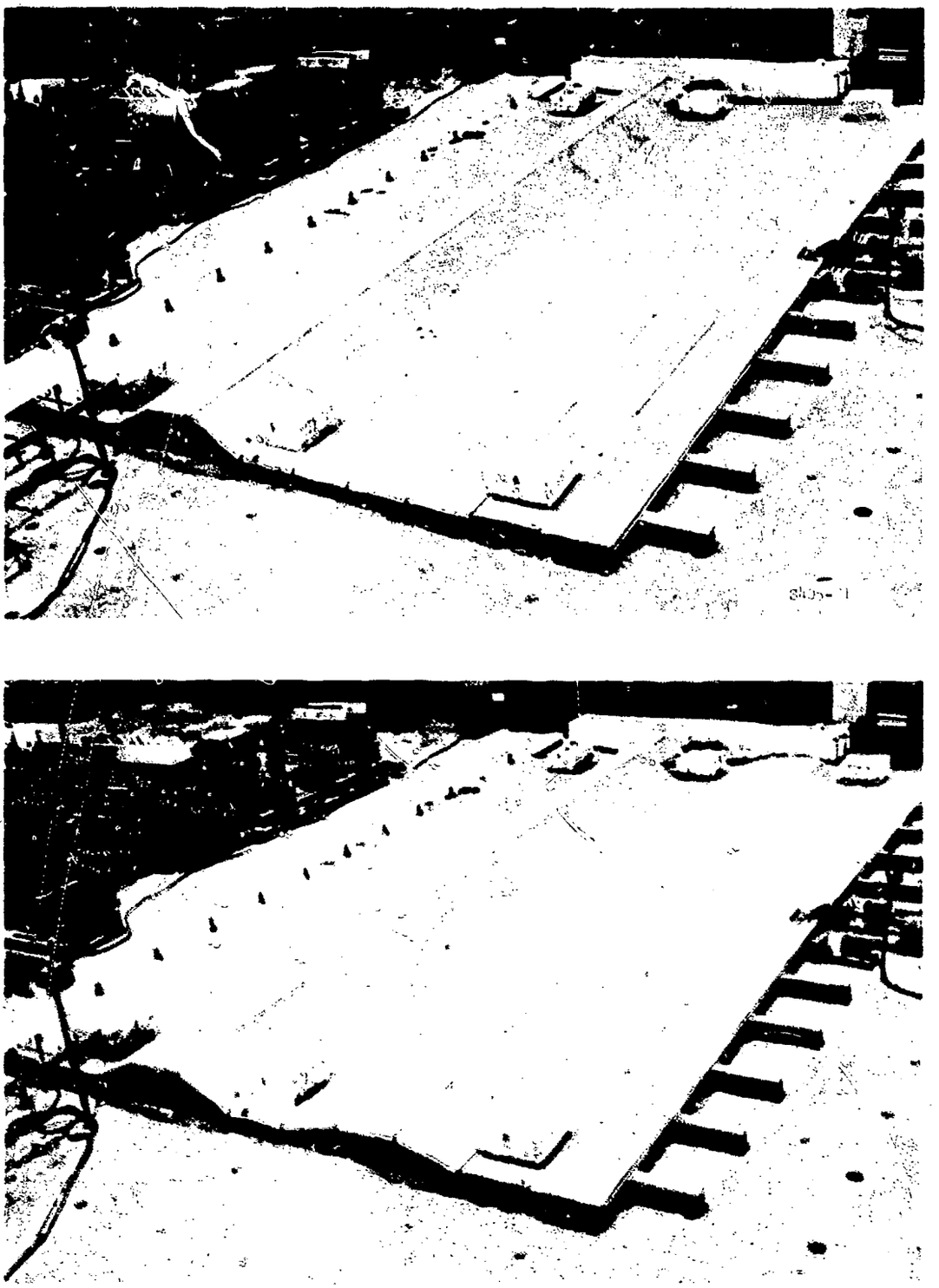

Figure 21 Buckled surface of 36-ft-wide XM18 mats, with load blocks

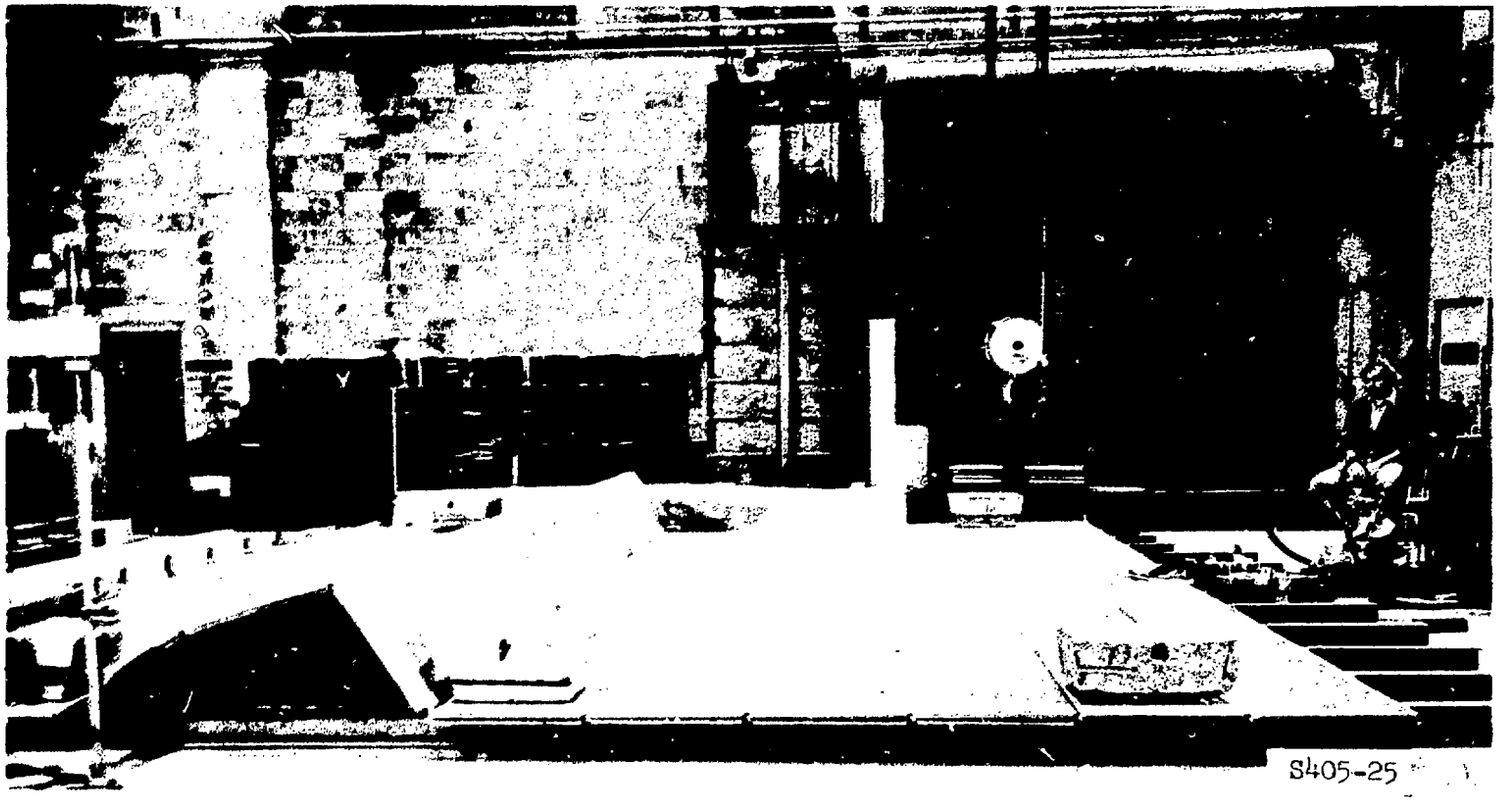

Figure 22. Buckled surface of XM18 mats, failure of joints incipient, 36 ft wide

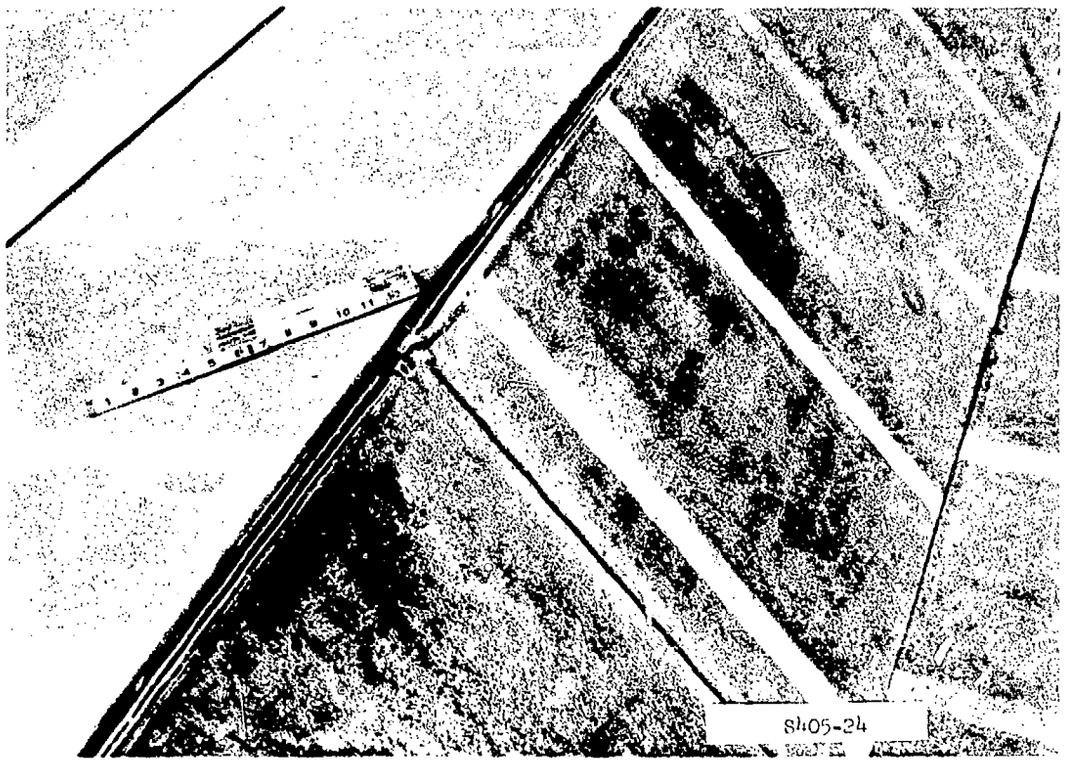

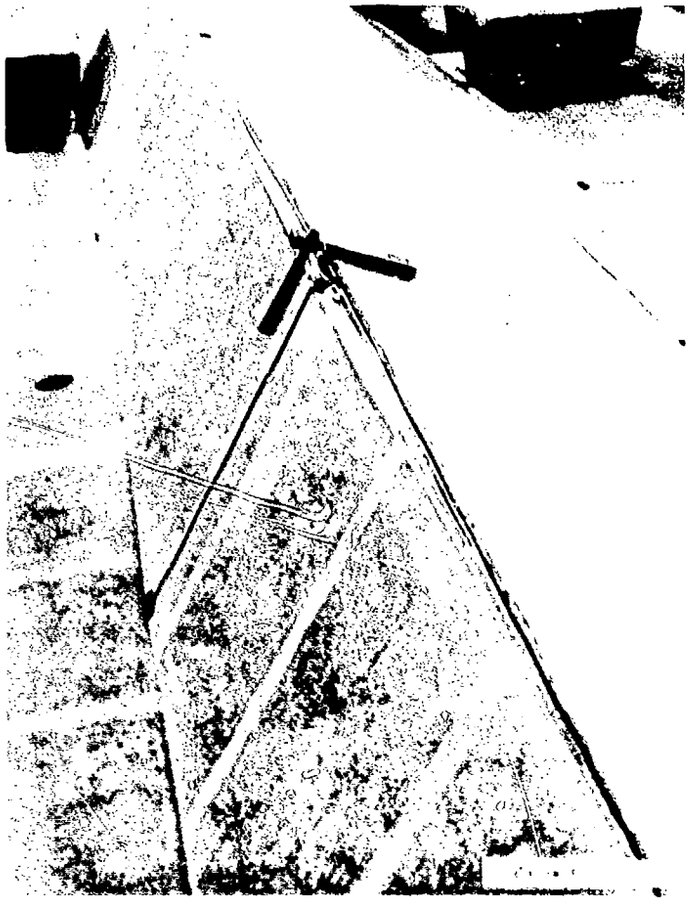

Figure 23. Close-ups of failed joint due to buckling XM18 mats

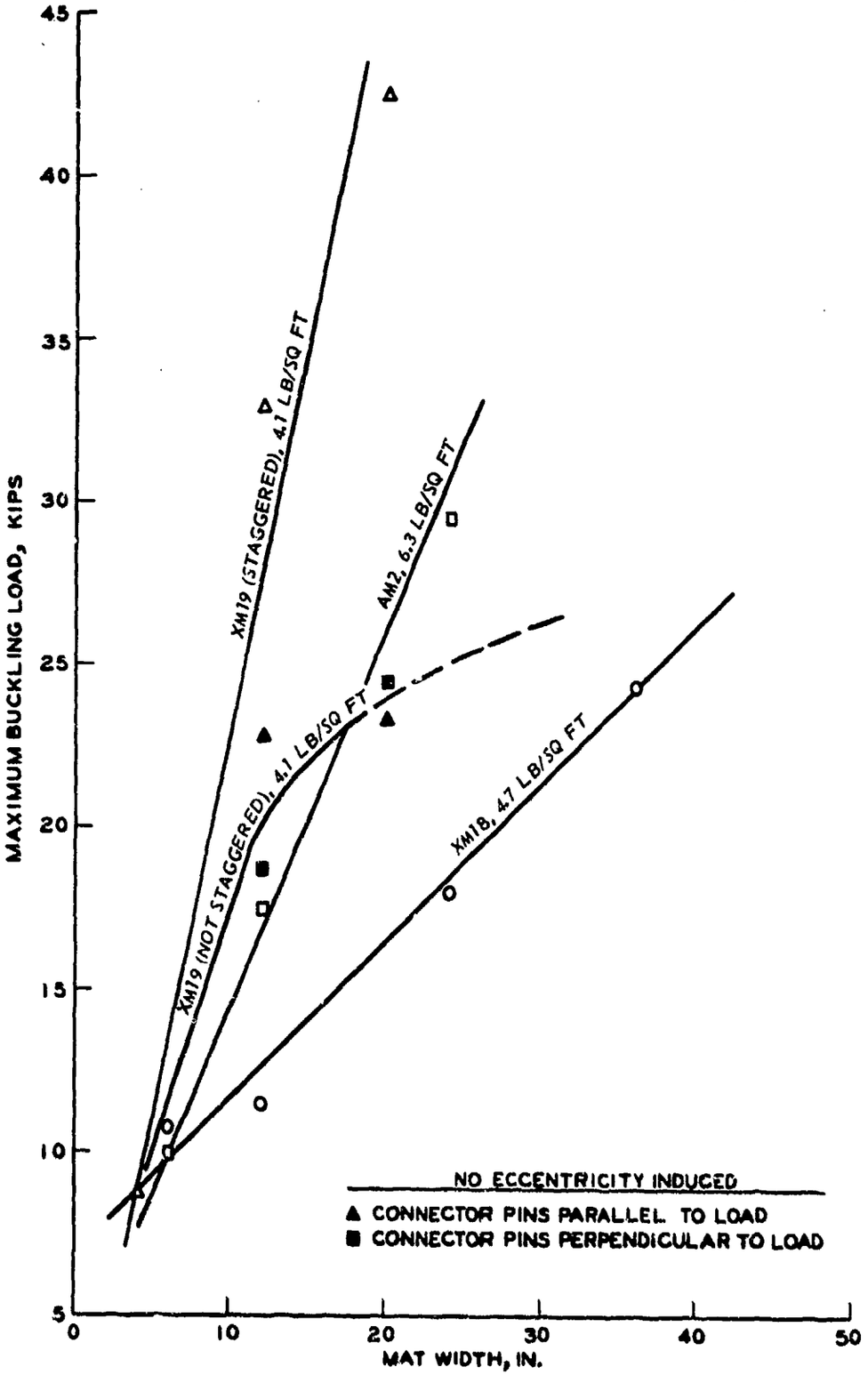

Figure 24. Relationship of buckling loads and mat width for different mats

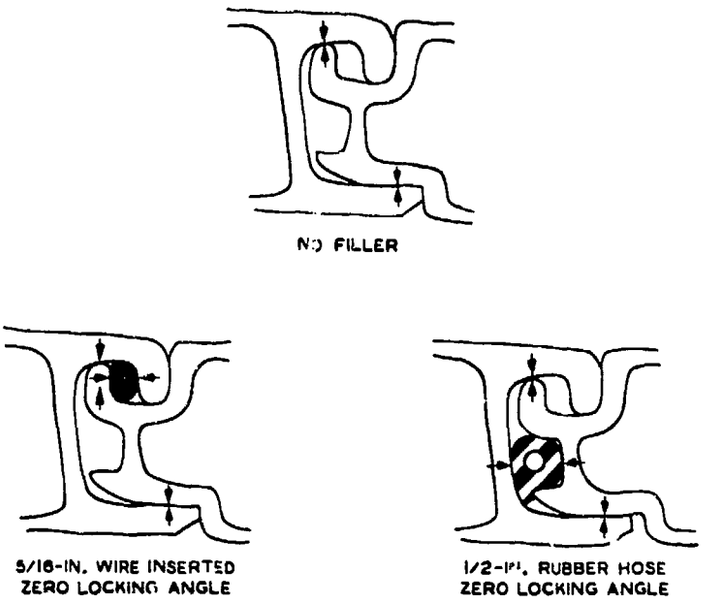

Figure 25. Configurations of XM18 mats with and without fillers during buckling

BUCKLING SHAPE

40. As noted earlier in this report there is a difference in the buckled shape depending on the type of mat, the lay pattern, or the joint locking angle. In the tests it was also observed that the stability of the buckled form relative to its horizontal position along the mat depended on the buckled shape of the mat. The stability of the buckled shape has significance with respect to the ability of the buckling wave to move ahead of a rolling aircraft. All the evidence indicates the wave which formed ahead of the C-5A at Dyess AFB was a stable type which would not move horizontally ahead of the aircraft. As can be noted in the movies and photos which were taken of the failure, complete disintegration of the mat occurred when the aircraft ran onto the buckled mat. Disintegration was not caused by the horizontal braking of the aircraft.

41. The ability of the wave formed by buckling to move ahead of an aircraft depends not only on the shape of the wave but also on the speed of the aircraft and the height of the wave. Thus any statement regarding the ability of an unstable wave, such as the wave formed by the buckled XM19, to run ahead of a landing aircraft would be pure conjecture. About the only statement that can be made at this time is that a wave such as that formed by the buckling of AM2 or XM18 will not move ahead of an aircraft. However, it is possible that the wave formed by the buckling of the XM19 mat, or by other mats with insertions, may move ahead of the aircraft and roll without causing a mat failure.

PART V: FACTORS AFFECTING PERFORMANCE OF MATS DURING LANDING OPERATIONS

42. The forces imposed on a mat runway due to aircraft landing and braking are indicated in Figure 26. These forces are:

a. A normal component W due to the weight of the aircraft.

b. A friction force F_B between the tire and the mat which is proportional to the friction coefficient between the tire and the mat μ_t, the aircraft weight W, and the deceleration a.

c. A friction force F_S between the mat and the subgrade which is also proportional to aircraft weight as well as the coefficient of friction between the mat and subgrade μ_s

d. A tensile force F_T in the mat behind the aircraft.

e. A compressive force F_c in the mat ahead of the aircraft.

The maximum horizontal reaction of the mat system occurs when all joints behind the aircraft are fully extended while all joints ahead are compressed. To reduce the compressive force ahead of the aircraft, which contributes to buckling, it is desirable that as much tensile resistance be mobilized as possible. This can be accomplished if the joints of the system are maintained in a fully extended position. The insertions shown in Figure 25 would assist in keeping the joints in a state capable of resisting tension without requiring large horizontal displacements. In addition, the surface of the buckled mats is smoother and more continuous with the insertions because the locking angles of the mat are reduced. This would result in a configuration which would be more likely to move ahead of an aircraft without causing mat failure.

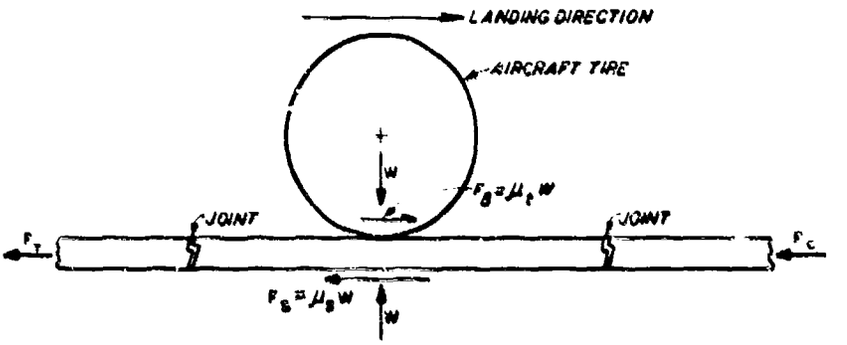

Figure 26. Forces on mat runway

43. Test results indicate that the buckling load is sensitive to the eccentricity of the mats. The effect of induced initial eccentricity in most cases was fairly pronounced for a narrow system but was obscured as the system width increased. It is easier for a 4- or 6-ft system to be laid flat and straight; a wider system would have a larger number of natural irregularities (i.e., warped panels, crooked or damaged joints, etc.) which would overshadow the effects of the induced eccentricity. Nevertheless, test results indicate that the runway subgrade should be as smooth as possible before laying mats.

44. The effect of panel width on buckling load is evident from the results of the tests of XM19 mat with joints not staggered. To use the available AM2 and XM18 mats, the alternative pattern shown in Figure 27 would increase the buckling load since the longitudinal joints of the XM19 mat are compatible

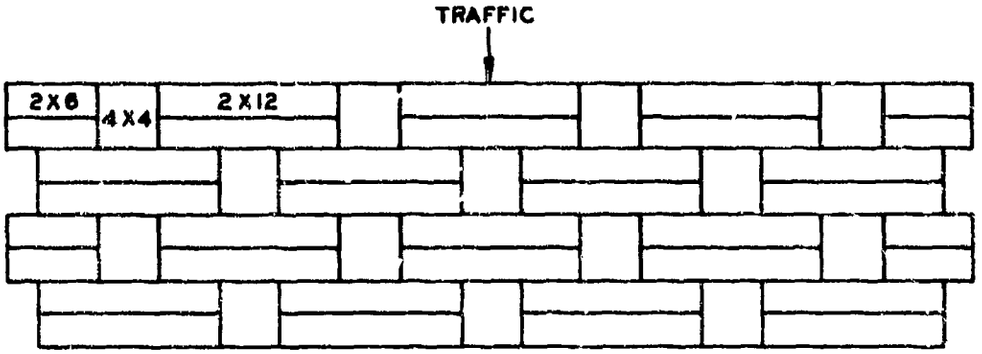

Figure 27. Lay pattern for AM2 or XM18 mat to increase effective panel width with XM19 panels

with those of the AM2 and XM18. This arrangement would make the AM2 and XM18 panels behave more like the XM19 with continuous transverse joints and with connector bars parallel (Figure 9) to traffic. However, the increase of the buckling load is believed to be not very significant.

45. The lay pattern shown in Figure 28 for AM2 and XM18 mats can increase the buckling load. Special rods and panels placed at the center of the runway will have to be manufactured. Because the mats are placed at 45-deg angles to the center rods, the component force parallel to the connector pins is reduced. The other component force will not cause the mats to shift because the mats are laid symmetrically with respect to the center rods.

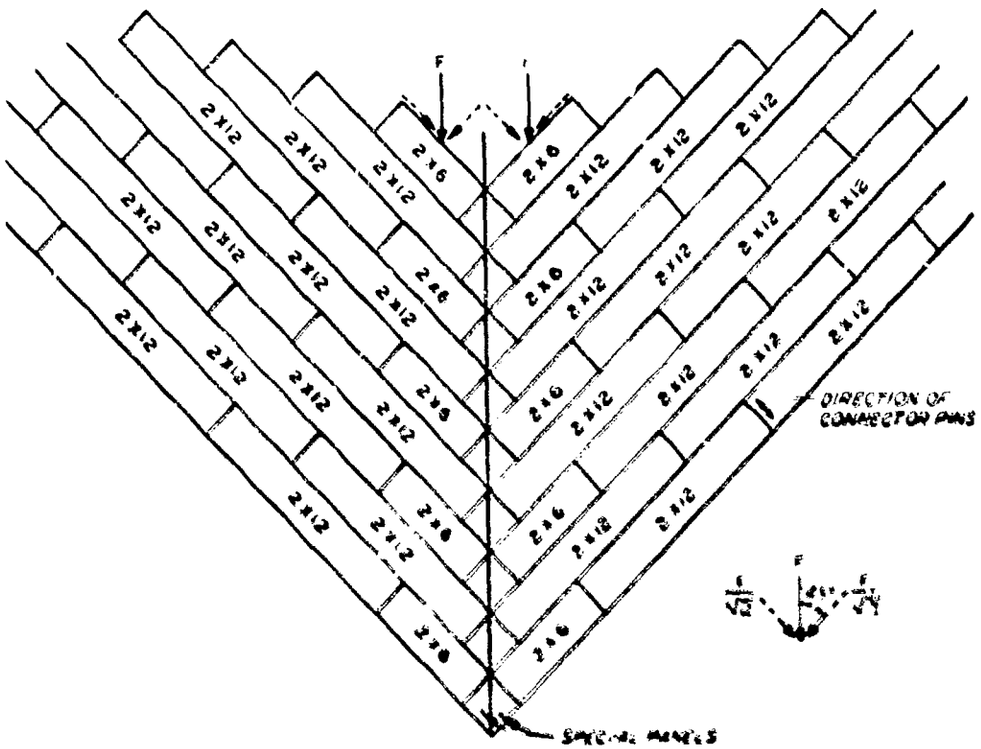

Figure 28. Lay pattern for AM2 and XM18 mats to increase the buckling load

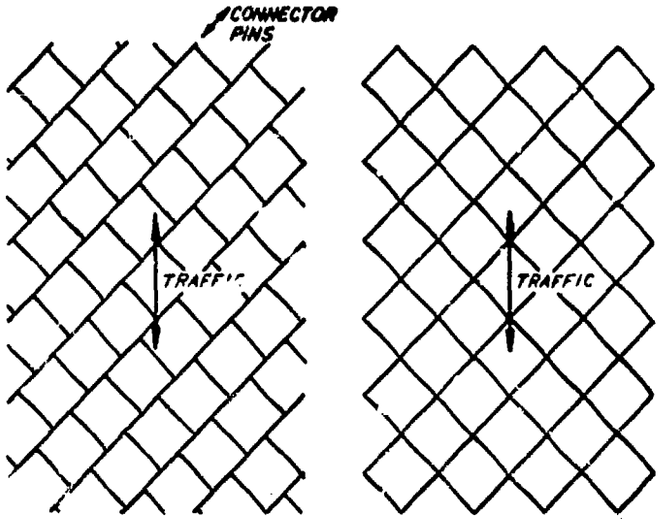

Figure 29. Diagonal lay patterns for XM19 mats

46. The lay patterns for XM19 mat shown in Figure 29 may increase the buckling load to some extent. The checkerboard pattern is more continuous but predominant migration is unidirectional and parallel to connector pins. In the diamond pattern the migration problem may be less severe but the system has a predominant weak axis parallel to the connector bars.

47. Test results indicate that edge restraints, either weights or anchors, are effective in increasing the buckling load when the load is applied near the edge. However, it is believed that this effectiveness would diminish very rapidly with distance from the edge and would not provide much benefit to the center portion of the mats.

PART VI: MATHEMATICAL ANALYSIS OF LANDING MATS

48. The results of static tests of various mat systems have been replotted in Figures 30-32. In Figure 30 the buckling load has been normalized with respect to mat width and total system weight.

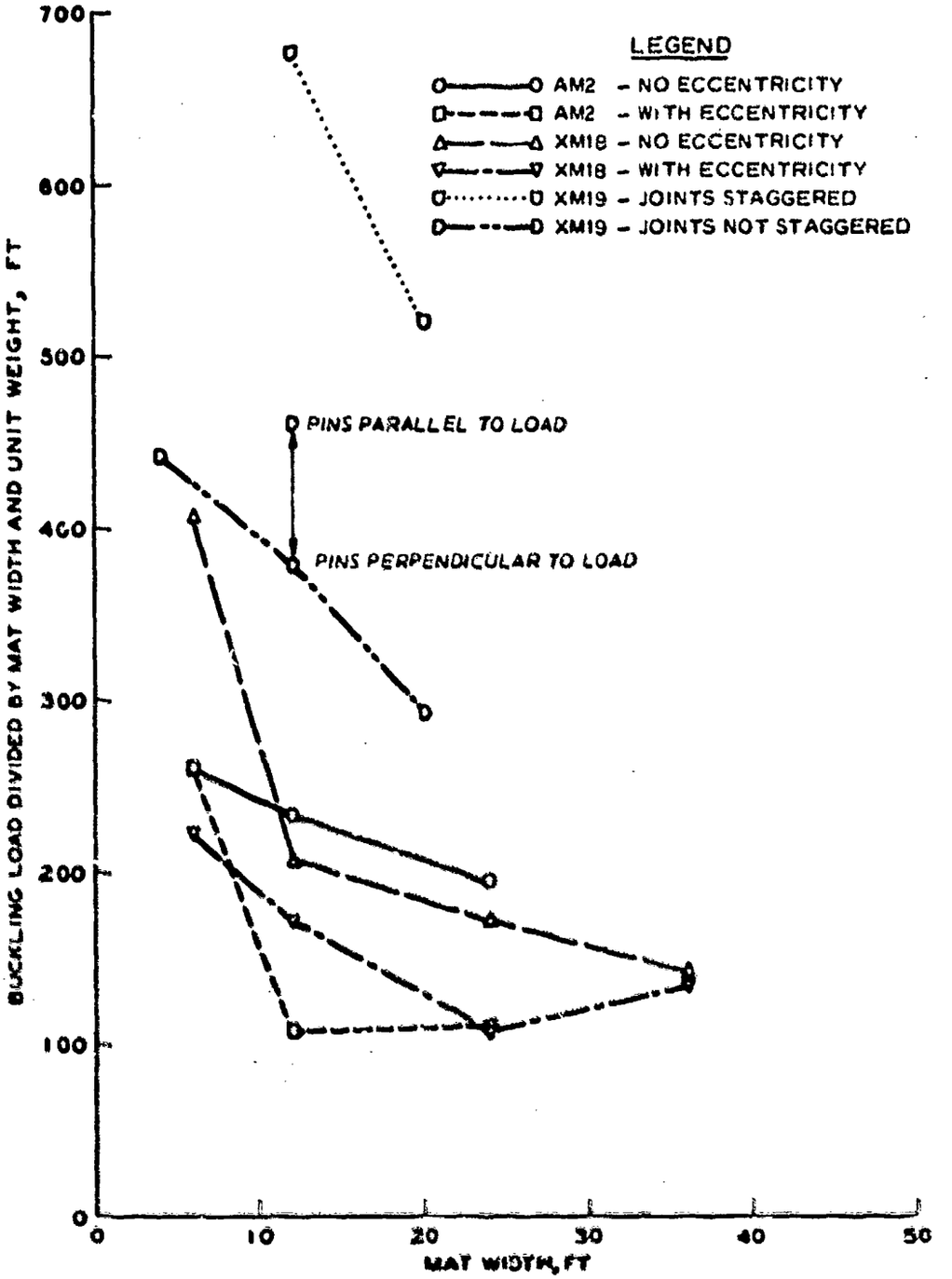

Figure 30. Normalized buckling load versus mat width

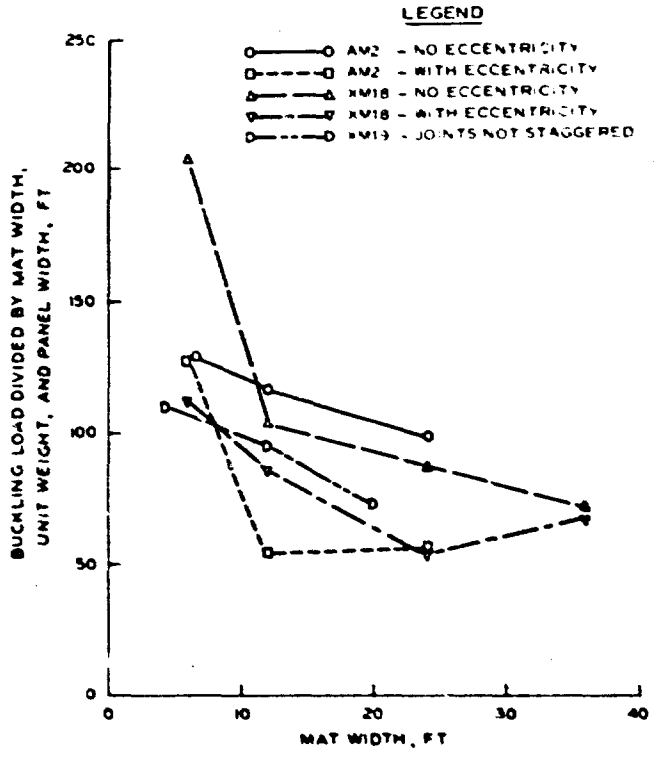

Figure 31. Normalized buckling load versus mat width

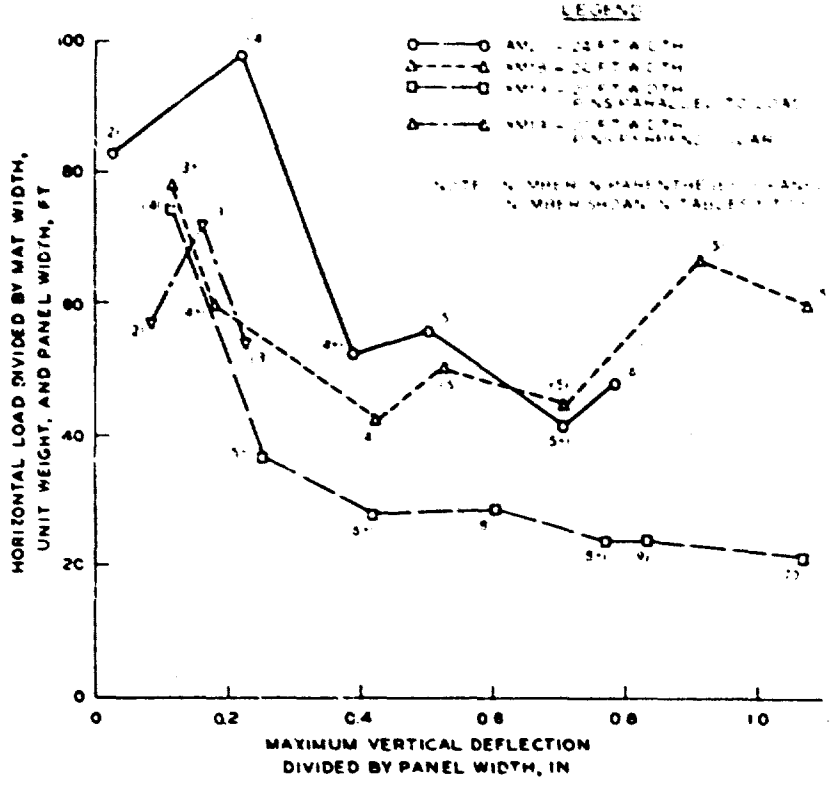

Figure 32. Normalized horizontal load versus normalized vertical deflection

This plot indicates the beneficial effect of panel width (4 ft for XM19, 2 ft for AM2 and XM18) on buckling load. In Figure 31 the buckling load has been further normalized with respect to panel width. The curves of Figure 31 indicate that the nondimensional buckling load is relatively independent of system width within the range of widths tested.

49. The variation of the nondimensional horizontal load on the mat with vertical deflection is illustrated in Figure 32 for several mat systems. These curves indicate that the maximum horizontal reaction of the mat is attained at low vertical displacements and as soon as vertical displacement is initiated, the horizontal load required to induce further deflection diminishes to essentially a constant value and additional imposed horizontal deformation results only in increasing the number of panels undergoing vertical displacement during the buckling process.

50. Except for the XM19 mat with staggered joints, the behavior of all mats tested may be demonstrated by a simplified articulated system composed of straight rigid bars and moment-free (frictionless) joints as shown in Figure 33a. Once buckling of the real mat system was initiated, the buckled shape progressed through the series of configurations shown in Figure 33b-f.

51. For the configuration shown in Figure 33, the nondimensional horizontal load, Q, required to sustain each of the buckled shapes may be expressed as

$$Q = \frac{3 - (-1)^n}{4} \cot\left[\frac{3 - (-1)^n}{4}\,\theta\right]$$

and the maximum nondimensional vertical displacement Δ (maximum displacement divided by panel width) is

$$\Delta = \sin\left[\frac{3 - (-1)^n}{4} \cdot \theta\right] + \sum_{i=1}^{2} J_i \cdot \sin\left\{\arctan\left[\frac{4i + 1 + (-1)^n}{4}\right] \cdot \tan\left[\frac{3 - (-1)^n}{4} \cdot \theta\right]\right\}$$

where

θ = angle shown in Figure 33

n = number of panels in buckled shapes

$J_i = 0$ for $n < 4$

$J_1 = 1$ for $n \geq 4$

$J_2 = 0$ for $n < 6$

$J_2 = 1$ for $n = 6$

Plots of Q versus Δ are shown in Figure 34 for values of the angle θ, Figure 33, up to 10 deg. Nondimensional potential energy of the system weight (weight potential energy divided by total system weight) as a function of maximum vertical displacement is shown in Figure 35.

52. The straight mat shown in Figure 33a is capable of transmitting any level of horizontal load.

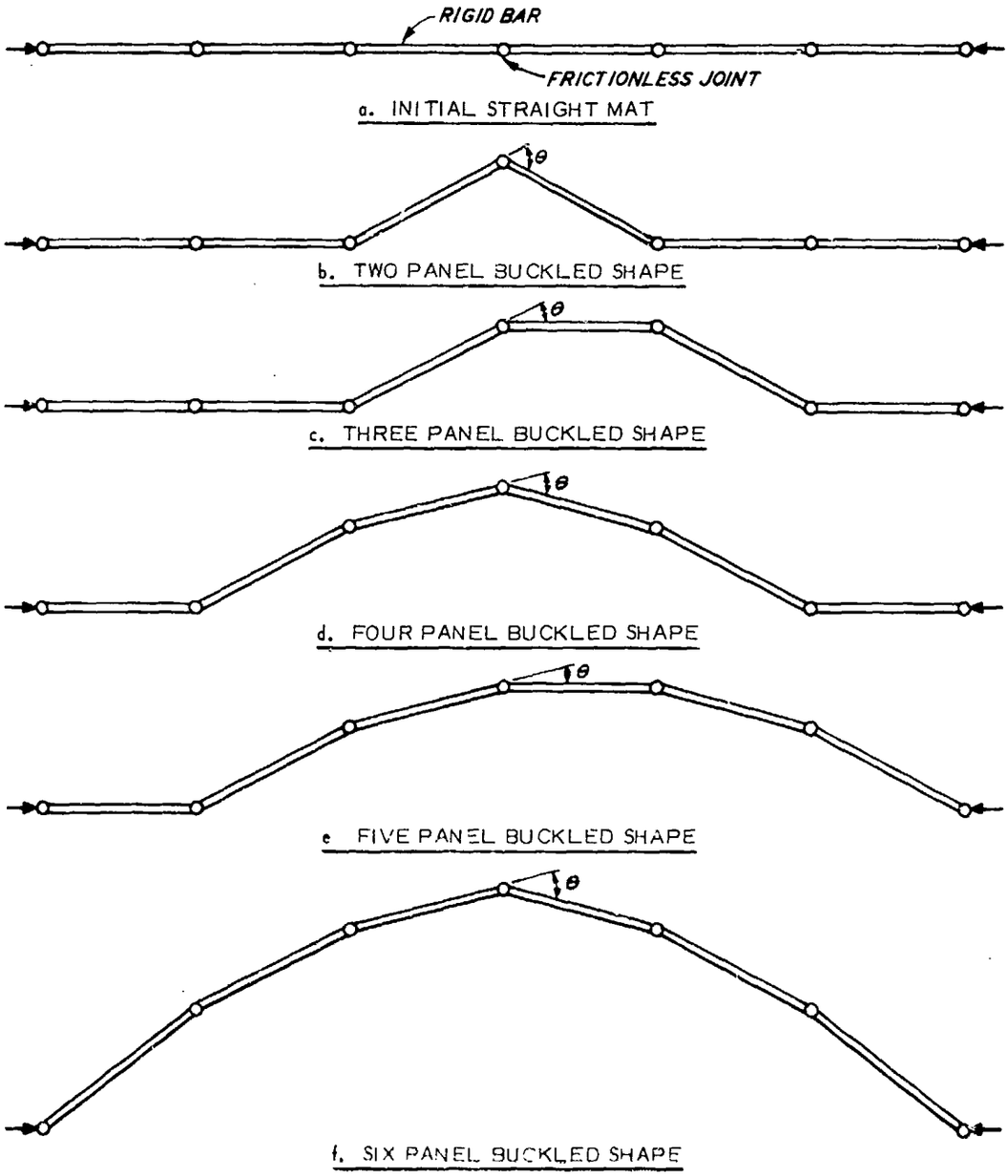

Figure 33. Buckled configurations of idealized mat

However, if any initial vertical displacement consistent with one of the displaced shapes of Figure 33b-f is present, then the horizontal load necessary to sustain the system in equilibrium decreases rapidly as the deflection increases.

53. The joints of the real mat are relatively moment free, as assumed in the idealized system, only up to a limiting value of the angle θ. This limiting value, referred to as the "locking angle" above, depends on the type of mat and the condition of the joints and has been observed to range from approximately 4 to 10 deg. When θ reaches the locking angle at a joint, then that joint is no longer

moment free and the horizontal load required to induce further vertical deflection increases rapidly depending on the stiffness of the joint. This is illustrated by the dashed vertical lines in Figure 34 for a locking angle of 5 deg. Up to this value of displacement, the total potential energy of the system is essentially equal to the potential energy of the system weight. When the locking angle is reached any additional work done on the system is stored as strain energy in the locked joint and the total energy of the system increases with little change in the weight potential energy. This increase is illustrated by the arrows in Figure 35 for a locking angle of 5 deg.

54. It is now possible to obtain a qualitative visualization of the buckling phenomena observed in tests of the real mat. Although the real mat was initially flat before loading, there existed myriad natural irregularities in the system. These irregularities provide the vertical displacements required to begin buckling. As horizontal load was applied to the system, the total potential energy of the system increased with the work done on the system being stored as axial strain energy due to the axial flexibility of the real mat panels. As the load and energy increased above the values consistent with those of the initial state, the initial state became unstable and the system underwent a sudden transition to a new configuration at a higher vertical displacement and an attendant reduction of load necessary to sustain equilibrium in the new shape. When additional horizontal loading effort was applied to the system, the vertical deflection increased, accompanied by decreasing horizontal load and increasing weight potential energy until the locking angle at a joint was again reached. When joint locking occurred, the load required for further displacement increased due to the moment resistance developed in the locked joint and the total potential energy of the system increased. The increased energy in the system was stored as strain energy in the locked joint. When the horizontal load and total energy in the current state reached sufficiently high levels, the system again became unstable and progressed to a new configuration with an accompanying decrease in axial load, increase in vertical deflection, and increase in the number of panels comprising the buckled shape. This process was repeated as the buckled system moved progressively through the shapes shown in Figure 33. Illustrative variations in loads, displacement, and energy during the buckling process are shown in Figures 36 and 37 by the heavy curves. The similarity between the speculative load-displacement behavior shown in Figure 36 and the observed behavior of the real system, Figure 32, is apparent.

55. Because the joints of the real mat are not moment free before locking, and due to shifts in the points of horizontal load transfer through the joint during buckling (see Figure 8), only qualitative comparisons between the idealized and real systems are available. However, it is possible to draw several conclusions which apply to an assessment of the compressive load transfer capabilities of the real mat.

a. The horizontal load at which buckling will begin depends almost exclusively on the vertical eccentricities existing in the mat at the time the load is applied. Because of the random nature of initial irregularities of the real system (e.g., warped panels, damaged joints, uneven subgrade) the initial buckling load is an unreliable measure of the load-carrying capacity of the system.

b. Once buckling has begun, the horizontal resistance of the mat diminishes rapidly and attains a relatively constant value even though the system continues to displace vertically with progressively larger numbers of panels involved in the buckled shape.

c. The resistance of the mat to horizontal loads after buckling depends predominantly on the locking angle at the joint. The postbuckling resistance capability of the mat increases rapidly with decreased locking angle (see Figure 34).

d. The number of panels involved in the buckled shape increases with reduced locking angle. Even though the vertical displacement increases with the number of panels, the profile of

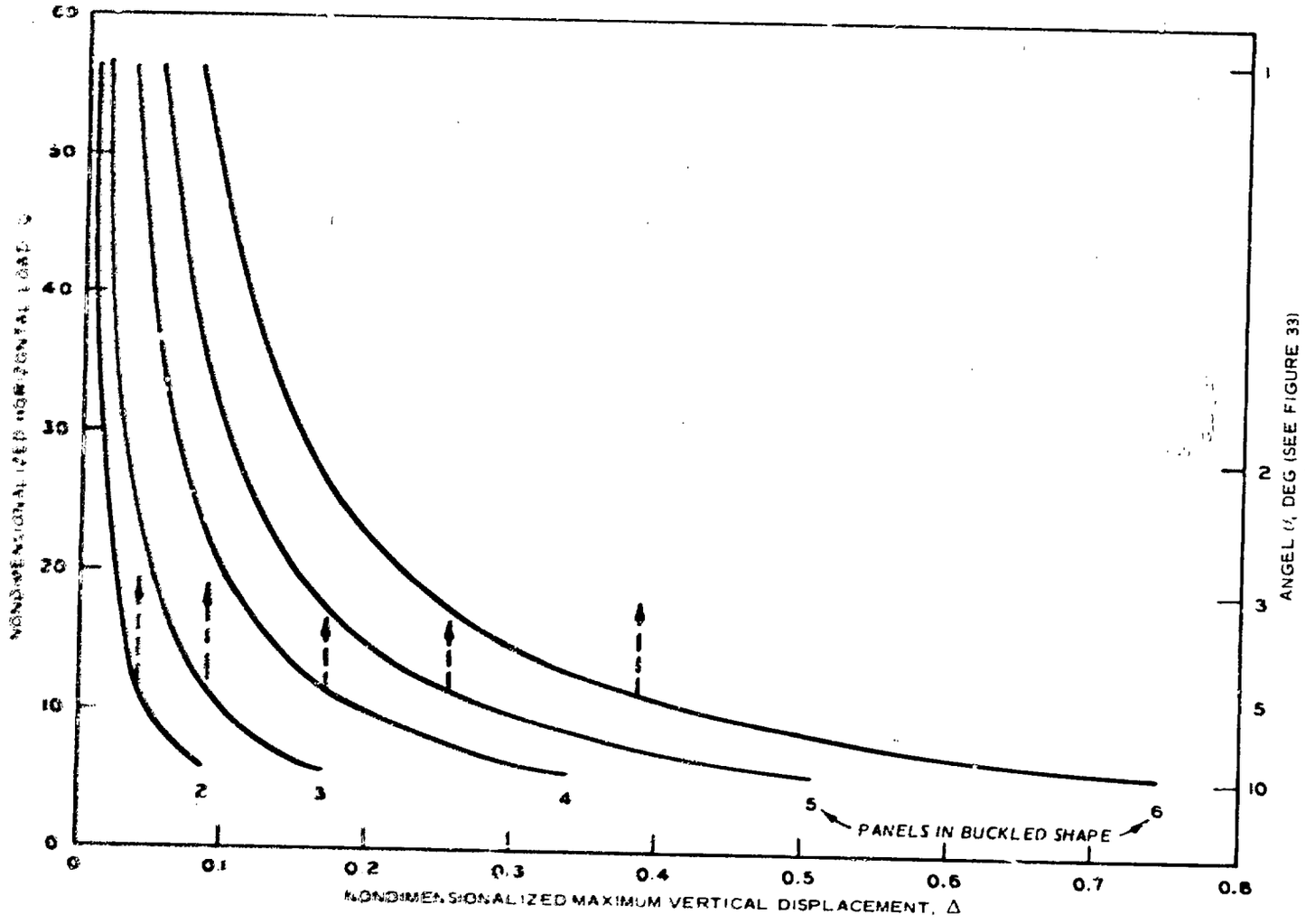

Figure 34 Horizontal load versus vertical displacement for various buckled configurations of idealized mat

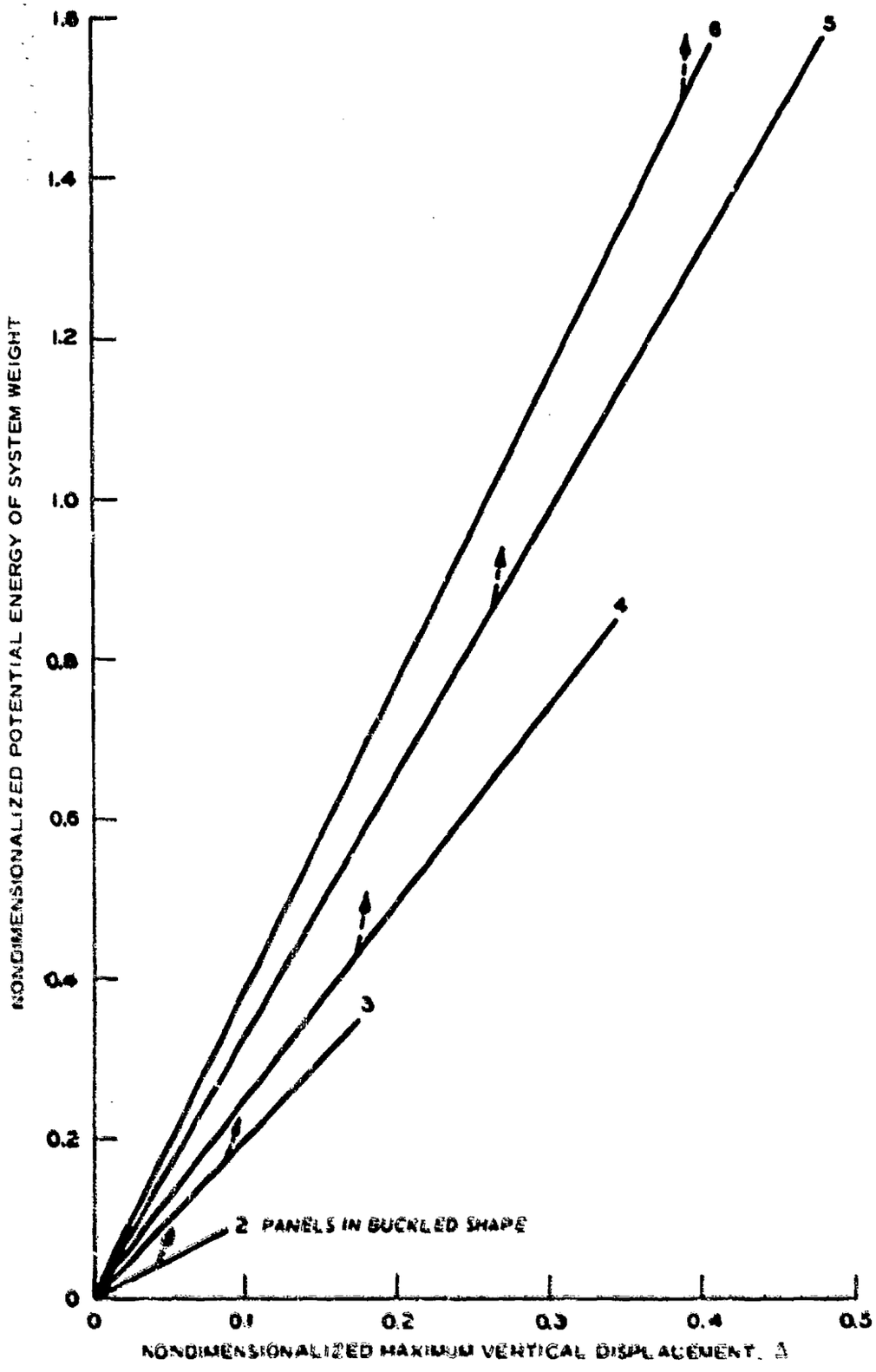

ure 35 Potential energy of system weight versus vertical displacement for buckled shapes of idealized mat

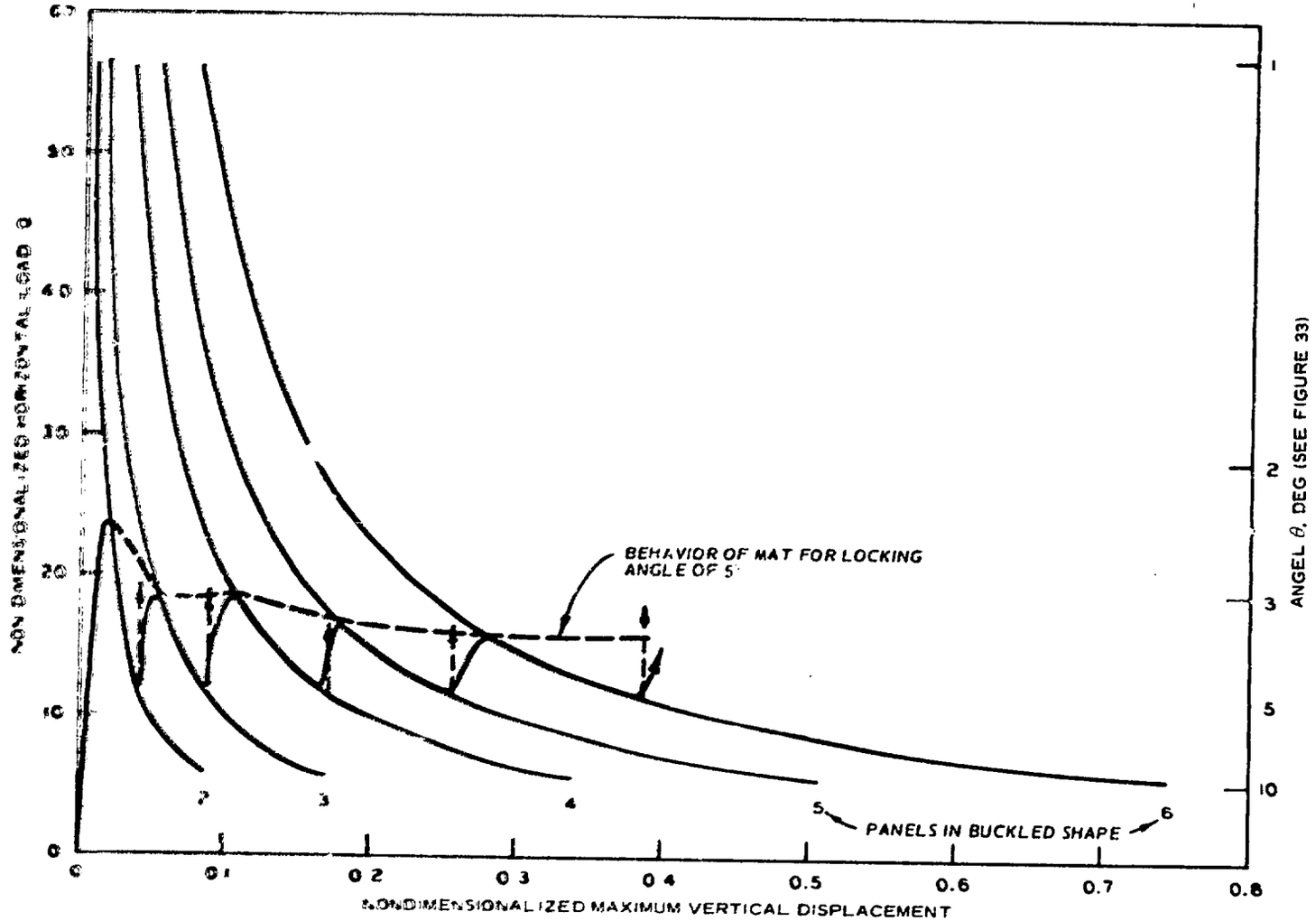

Figure 36. Horizontal load versus vertical displacement for various buckled configurations of idealized mat

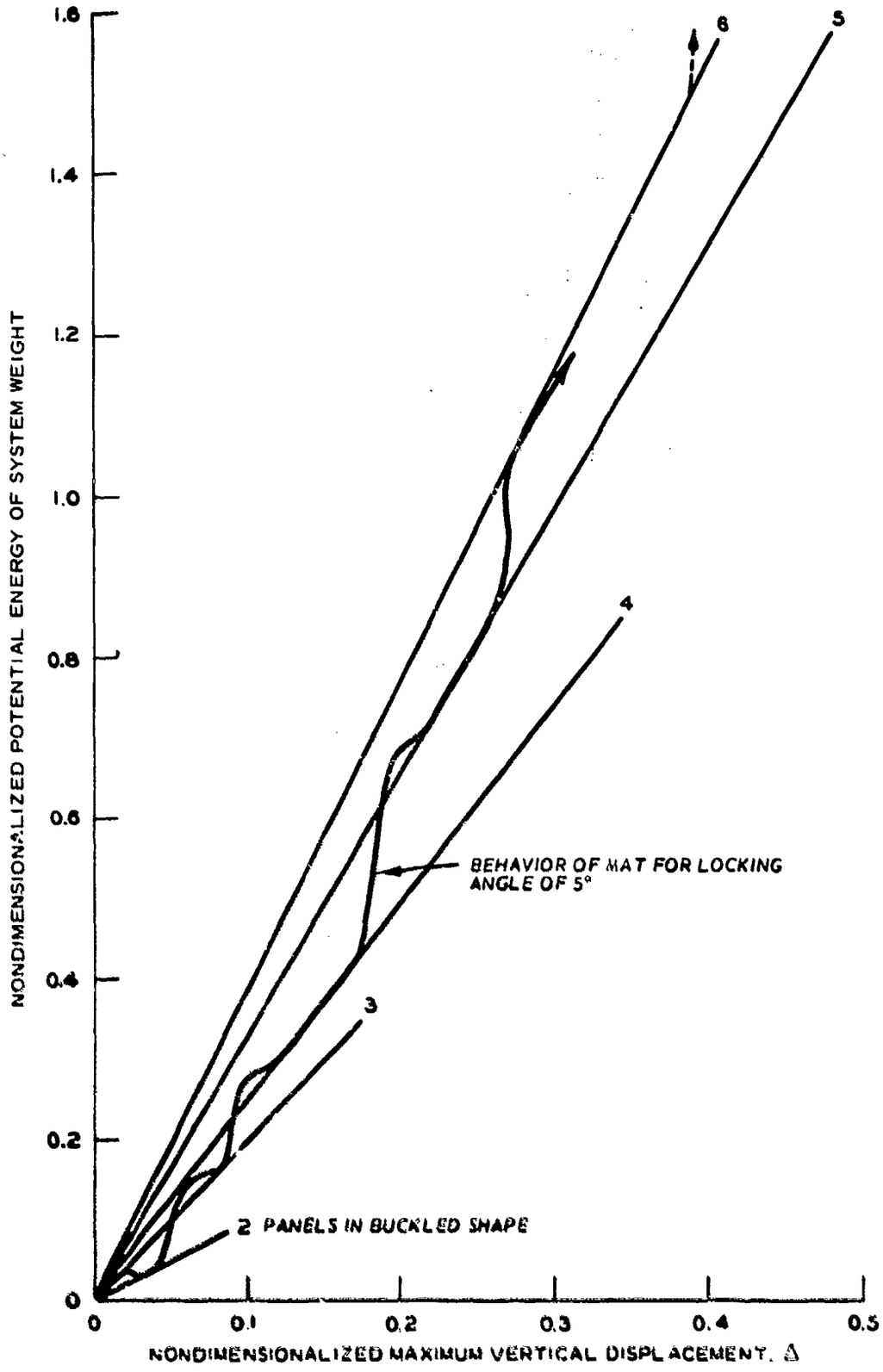

Figure 37 Potential energy of system weight versus vertical displacement for buckled shapes of idealized mat. Variations shown by heavy curve

the buckled shape presented to a landing aircraft is longer and smoother than that for a low number of panels and offers the possibility that the buckled shape will move ahead of the aircraft.

e. Because of the random nature of irregularities in the real system, there appears to be little benefit to be gained from more elaborate mathematical analyses directed toward a more exact determination of initial buckling load or of sustained postbuckling resistance.

PART VII: CONCLUSIONS AND RECOMMENDATIONS

CONCLUSIONS

Laboratory Buckling Tests

56. Because the available data are limited, it is only possible to present the following qualitative conclusions:

a. The initial buckling load of the mat increases with panel width, mat unit weight, and system width.

b. The initial buckling load of the mat decreases rapidly with increased initial eccentricities in the system.

c. The initial buckling load is independent of the locking angle of the joints.

d. The postbuckling resistance of the mat is substantially lower than the initial buckling load and increases rapidly with decreased locking angle.

e. The profile of the buckled wave becomes smoother and more continuous as the locking angle is reduced.

f. Insertion of filler rods in the joints perpendicular to the loading direction reduces the locking angle and in addition maintains the joints in a fully extended position to permit maximum mobilization of the tensile resistance of the mat behind a landing aircraft.

g. Any revision such as resilient filler insertions or alternative lay patterns which cause the mat to tend toward a continuous system or which increase the effective panel width will enhance the postbuckling behavior and may increase the initial buckling load.

Theoretical Analysis

57. As previously mentioned, because of the random nature of initial irregularities of the real system (e.g., warped panels, damaged joints, uneven subgrade) the initial buckling load is an unreliable measure of the load-carrying capacity of the system; more elaborate deterministic mathematical analyses directed toward a more exact determination of initial buckling load or of sustained postbuckling resistance are unwarranted.

RECOMMENDATIONS

58. To investigate the potential enhancement of mat behavior without requiring extensive revision of panel design, the following experimental investigations are recommended:

a. The smoother profile of a buckled mat with filler rods inserted in the joints may permit the buckled wave to propagate along the mat when it is encountered by the wheel. This possibility should be examined using the C-5A wheel assembly with a relatively large mat layout.

b. The alternative mat layout shown in Figure 27 is a relatively expedient means of increasing the effective panel width. The behavior of this layout should be examined in a series of tests similar to those reported above.

c. The diagonal lay patterns for XM19 mat shown in Figure 29 may increase the effective panel width while reducing the component of horizontal load perpendicular to the predominant weak joint (without connector pins). The behavior of these alternatives should be examined experimentally both with and without filler insertions in the weak joints.

REFERENCES

1. Green, H. L., "Observation of C-5A Operations on Landing Mat Test Facility, Dyess Air Force Base, Texas," Miscellaneous Paper S-72-10, Mar 1972, U. S. Army Engineer Waterways Experiment Station, CE, Vicksburg, Miss.
2. Carr, G. L., "Skid Tests on XM18, XM19, and T11 Landing Mats Placed in Contact with Soil and Placed on Membrane on Soil," Memorandum for Record, 27 Feb 1973, U. S. Army Engineer Waterways Experiment Station, CE, Vicksburg, Miss.
3. Kiefer, F. W., Blotter, P. T., and Christiansen, V. T., "Model Study of C-5A Landings on AM2 Landing Mat," Technical Report No. AFWL-TR-72-210, Aug 1973, Air Force Weapons Laboratory, Kirtland Air Force Base, N. Mex.
4. ———————, "Model Study of C-5A Landings on Dow Truss Web Landing Mat," Technical Report S-75-3, 1975, Air Force Special Weapons Center (PMRB), Kirtland Air Force Base, N. Mex.
5. Brabston, W. N., "Evaluation of Three-Piece AM2 Aluminum Landing Mat," Miscellaneous Paper No. 4-886, Apr 1967, U. S. Army Engineer Waterways Experiment Station, CE, Vicksburg, Miss.
6. White, D. W. and Gerard, C. J., "Evaluation of Dow Chemical Extruded Aluminum Landing Mat (MX18E1)," Miscellaneous Paper S-69-51, Dec 1969, U. S. Army Engineer Waterways Experiment Station, CE, Vicksburg, Miss.
7. Heller, L. W., "Kaiser Landing Mat Failure Study (MX19)," Miscellaneous Paper No. 4-881, Mar 1967, U. S. Army Engineer Waterways Experiment Station, CE, Vicksburg, Miss.

Table 1

Test* Results of XM19 Square Mats With Connector Pins Perpendicular to the Load

Load, kips	Horizontal Movement, in.	Vertical Movement, in.											
		1	2	3	4	5	6	7	8	9	10	11	12
0	0	0	0	0	0	0	0	0	0	0	0	0	0
24.45	2.50	0	0	0	0	0	0	0	-0.06	3.84	6.48	5.46	0.12
12.00	3.50	0	0	0	0	-0.06	-0.06	1.68	8.52	12.60	12.24	7.62	0.48
9.15	5.00	0	0	0	0	-0.06	4.38	13.32	19.14	20.22	15.48	6.90	0.30
9.35	7.31	0	0	0	0.12	6.36	16.42	25.92	29.22	27.24	19.68	7.74	0.36
9.75	10.00	0	0	0.12	1.56	9.96	24.18	33.24	36.90	34.08	24.72	10.44	1.08
9.55	11.13	0	0.12	0.36	7.14	21.12	33.18	39.72	40.80	36.00	25.32	10.68	1.14
7.00	15.50	0	0.30	4.62	15.72	32.76	45.54	51.48	50.88	43.68	30.36	13.20	1.80

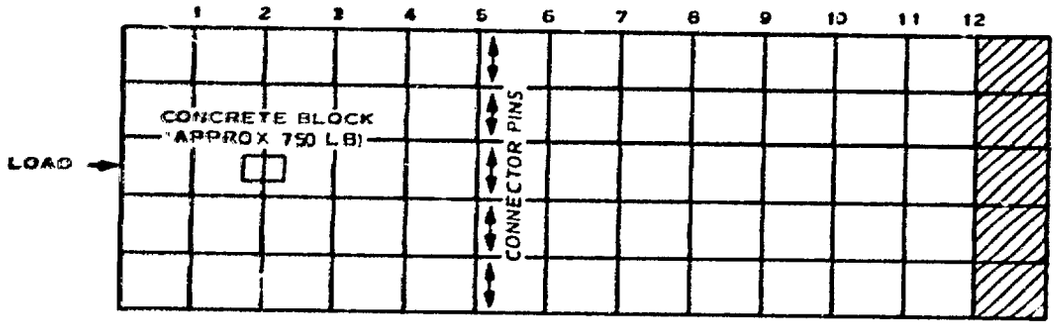

* Test No. 173-20-3: length 40 ft, width 20 ft; 4- by 4-ft XM19 mat; 5/12/73; zero eccentricity.

Table 2

Test* Results of XM19 Square Mats With Connector Pins Parallel to the Load

Load, kips	Horizontal Movement, in.	Vertical Movement, in.											
		1	2	3	4	5	6	7	8	9	10	11	12
0	0	0	0	0	0	0	0	0	0	0	0	0	0
15.00	3.00	0.00	0.12	0.06	0.06	0.12	0	0	4.02	0.12	0.06	-0.06	-0.24
25.00	4.00	0.06	0.12	0.06	0.06	0.12	0.06	0.06	7.38	7.68	0.18	-0.06	-0.18
17.50	5.00	0.00	0.12	0.06	0.06	0.12	0.06	0.30	10.50	10.92	0.30	-0.06	-0.24

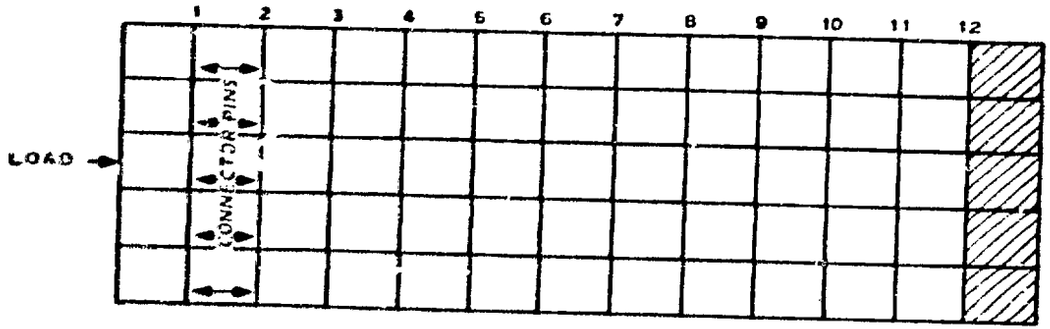

* Test No. 1-20-3: Length 40 ft, width 20 ft; 4- by 4-ft XM19 mat; 1/21/73; zero eccentricity.

Table 3

Test* Results of XM19 Square Mats With Connector Pins Perpendicular to the Load, Mats Staggered

Load, kips	Horizontal Movement, in.	Vertical Movement, in.											
		1	2	3	4	5	6	7	8	9	10	11	12
0	0	0	0	0	0	0	0	0	0	0	0	0	0
42.65	2.50	0.06	0	-0.12	-0.06	0.18	2.04	5.04	6.90	6.36	3.80	1.63	0
75.00	3.50	0.06	0	-0.12	1.08	4.92	10.02	13.92	14.64	11.58	6.60	2.58	0.06
111.20	4.88	0.06	-0.06	1.14	5.16	11.88	18.78	22.14	21.24	15.90	8.82	3.36	0.12

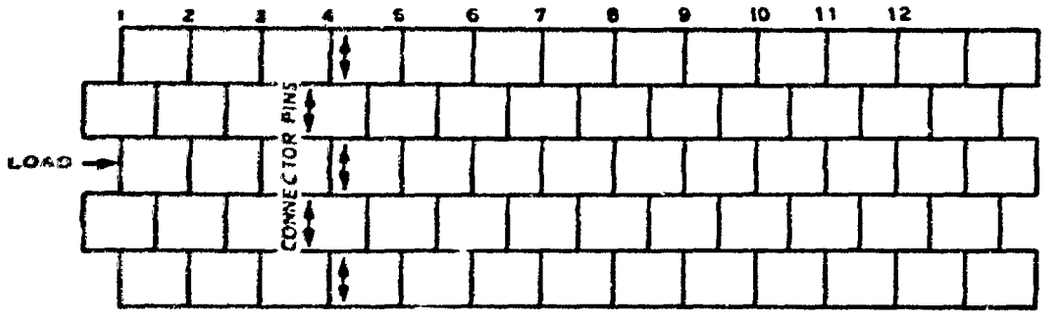

* Test No. 190-20-0: Length 40 ft, width 20 ft; 4- by 4-ft XM19 mat; 5/16/73; zero eccentricity.

Table 4

Test* Results of AM2 Mats, 24 ft Wide

Load, kips	Horizontal Movement, in.	Vertical Movement, in.										
		1	2	3	4	5	6	7	8	9	10	11
0	0	0	0	0	0	0	0	0	0	0	0	0
12.5	2.5	0	0.06	0	0	0	0	0	0.06	0	0.72	0.12
25.0	2.65	0	0.06	0	-0.06	0.18	0.6	0.18	0.06	-0.06	1.02	0.18
29.5	3.00	0	0.06	0	-0.06	4.62	5.34	3.9	0.24	-0.06	0.66	0.06
33.75	4.19	0	0.06	0.12	0.54	7.20	9.30	6.96	0.72	-0.06	0.78	0.12
16.85	5.00	0	0.06	0.06	6.96	12.06	11.94	7.56	0.54	-0.06	0	0
42.5	8.31	0	0.12	0.24	9.84	16.74	16.98	11.04	0.84	-0.06	.72	0.12
44.5	9.94	0	0.1	0.46	11.34	16.54	18.90	12.4	0.66	-0.06	0.78	0.12

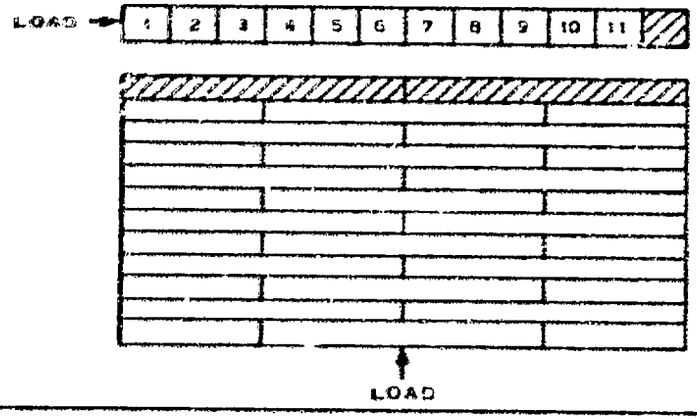

* Test No. D-1: length 22 ft, width 24 ft; 2- by 12-in AM2 mat; 1/61/73; zero eccentricity.

Table 5

Test* Results of XM18 Mats, 24 ft Wide

Load, kips	Horizontal Movement, in.	Vertical Movement, in.										
		1	2	3	4	5	6	7	8	9	10	11
0	0	0	0	0	0	0	0	0	0	0	0	0
12.5	2.56	0.06	0	0	0	-0.06	0	0.06	0.03	-0.06	0.12	0
17.69	2.63	0.06	0.06	0	0	0	0.06	1.26	2.82	1.08	0.18	-0.06
13.50	2.81	0.06	0.06	0	0	0	0.06	2.04	4.38	3.12	0.72	0.06
9.5	4.44	0.06	0.06	0	0	0	0.18	7.32	10.14	6.84	0.36	0
11.25	5.13	0.06	0	0	0	0	0.06	7.68	12.60	11.64	7.56	0.48
10.0	9.13	0.06	0.06	0	0	0	0.12	11.70	18.12	17.76	11.64	0.90
15.0	13.06	0.06	0.06	0	0	0	0.30	13.92	21.90	21.84	14.64	1.14
13.5	16.94	0.06	0	0	0	-0.06	0.30	15.84	25.86	24.48	15.84	1.26

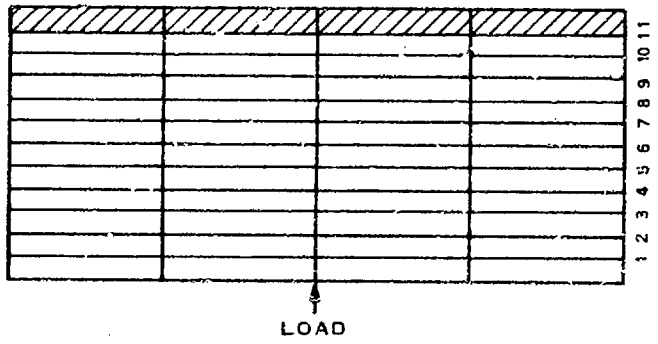

* Test No. G-1: length 22 ft, width 24 ft; 2- by 12-ft XM18 mat; 3/7/73; zero eccentricity.

APPENDIX A

AM2 LANDING MAT PERFORMANCE UNDER C-5A TRAFFIC AT DYESS AFB, TEXAS

DEPARTMENT OF THE ARMY
WATERWAYS EXPERIMENT STATION, CORPS OF ENGINEERS
P. O. BOX 631
VICKSBURG, MISSISSIPPI 39180

IN REPLY REFER TO: WESSF

3 November 1970

MEMORANDUM FOR RECORD

SUBJECT: AM2 Landing Mat Performance under C-5A Traffic at Dyess AFB, Texas

1. In a meeting with Mr. Ronald L. Hutchinson on 21 September 1970, Dr. Yu-Tang Chou and Dr. Walter R. Barker were requested to study the available information concerning the AM2 mat failure at Dyess AFB, Texas. The failure in question occurred on 24 August 1970 during a landing operation of a C-5A aircraft.

2. The available information on the events of the failure consisted in its entirety of the report by Mr. H. L. Green and a film taken by Mr. R. H. Ledbetter (selected frames are shown in Figure A1).

3. Information on the AM2 mat is available from reports of simulated-traffic investigations conducted by the Waterways Experiment Station (WES). The report covering the evaluation of May two-piece AM2 mat is given in Miscellaneous Paper S-68-11. One WES report (Miscellaneous Paper S-69-50) covers the reconstruction of the landing mat test facility and its performance during C-141A flight tests. Another report by the U. S. Army Test and Evaluation Command covers the performance of the mat at Dyess AFB from 15 August 1966 to 18 October 1967.

4. In order to obtain additional information concerning the behavior of the AM2 mat, several tests were conducted at WES by personnel of the Flexible Pavement Branch. The tests, which are described on pages A8 through A12, consisted of a tension test of the longitudinal joint (side joint), three buckling tests, and a test to determine the coefficient of friction beneath the mat. Figures A2, A3, A4-A8 (which are from the Ledbetter film), A9-A13, and Table A1 illustrate these tests. Additional tests are presently being conducted by personnel of the Mat Section, Expedient Surfaces Branch.

5. The horizontal thrust applied to the mat runway by a braking aircraft is a function of normal force, the coefficient of friction between the tire and mat, and the coefficient of friction between the mat and subgrade. The relationship may be expressed in equation form as

$$F_H = (C_1 + C_2) F_V$$

where

F_H is the horizontal thrust

C_1 is the coefficient of friction between the tire and mat

C_2 is the coefficient of friction between the mat and subgrade

F_V is the normal force (assumed to be weight of the aircraft)

a. First distress noted. (Dot is reference point at edge of runway)

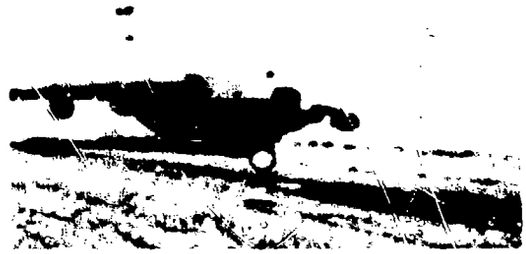

b. Bow wave starting to form

c. Bow wave completely blocking light beneath plane

d. Mat starting to come apart

e. Mat coming apart, light beginning to reappear

f. Plane past damage section of mat. One panel following plane

g. Plane taxiing out on runway

Figure 4.1. Sequence of photos made from motion picture film of mat failure

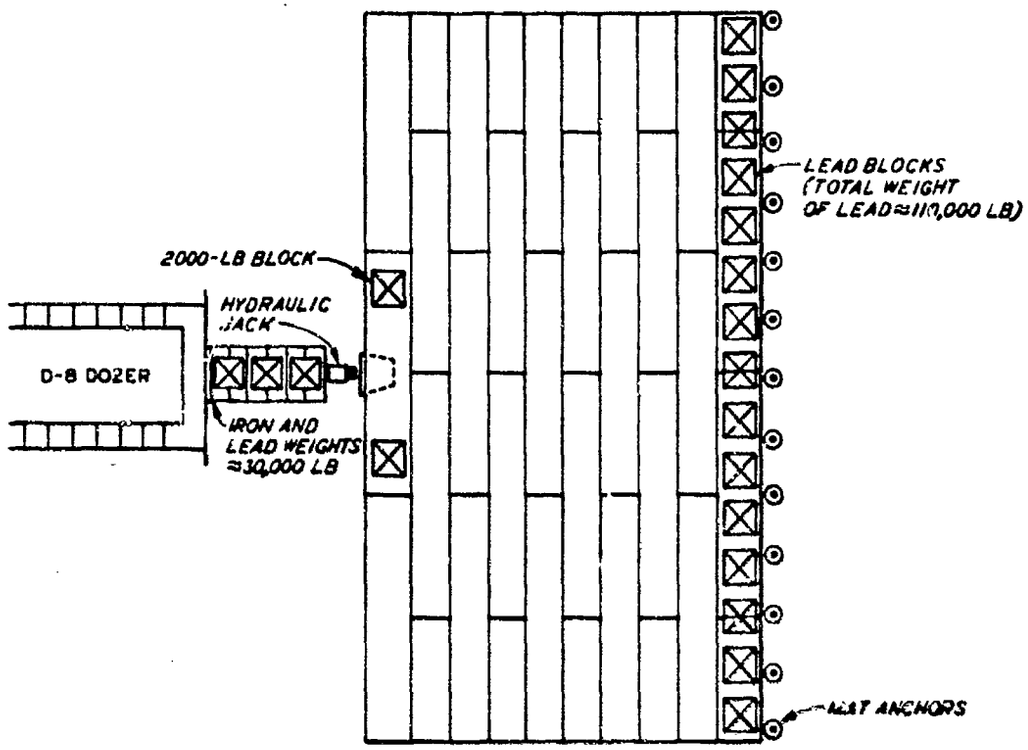

Figure A2 AM2 buckling Test No. 1, test layout of full section

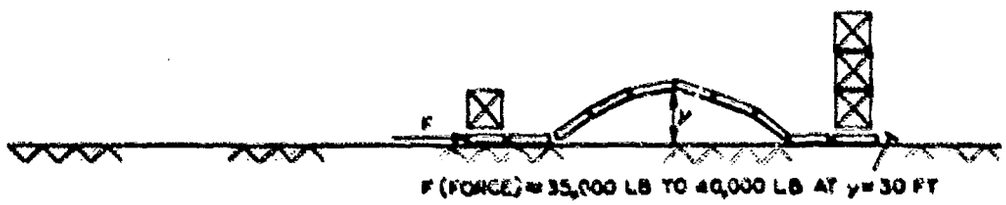

Figure A3 Final buckling mode for Test 1B

Previous tests of AM2 mat have indicated a maximum coefficient of friction between the tire and mat of 0.6. At Dyess the runways had been constructed using a membrane beneath the mat. The tests at Hangar 4 indicated the coefficient of friction between the mat and membrane to be 0.5. The weight of the aircraft at the time of landing was approximately 470,000 lb. Thus the horizontal thrust applied to the runways would be approximately 47,000 lb.

6. An examination of movies taken during the landing and mat failure at Dyess AFB shows a bow wave or buckling of the mat occurring in front of the aircraft's main landing gears. A bow wave involving some six to eight panels and obtaining a height of 3-4 ft is felt to have occurred. The tests conducted at Hangar 4 indicated that a horizontal thrust of approximately 40,000 to 60,000 lb would be necessary

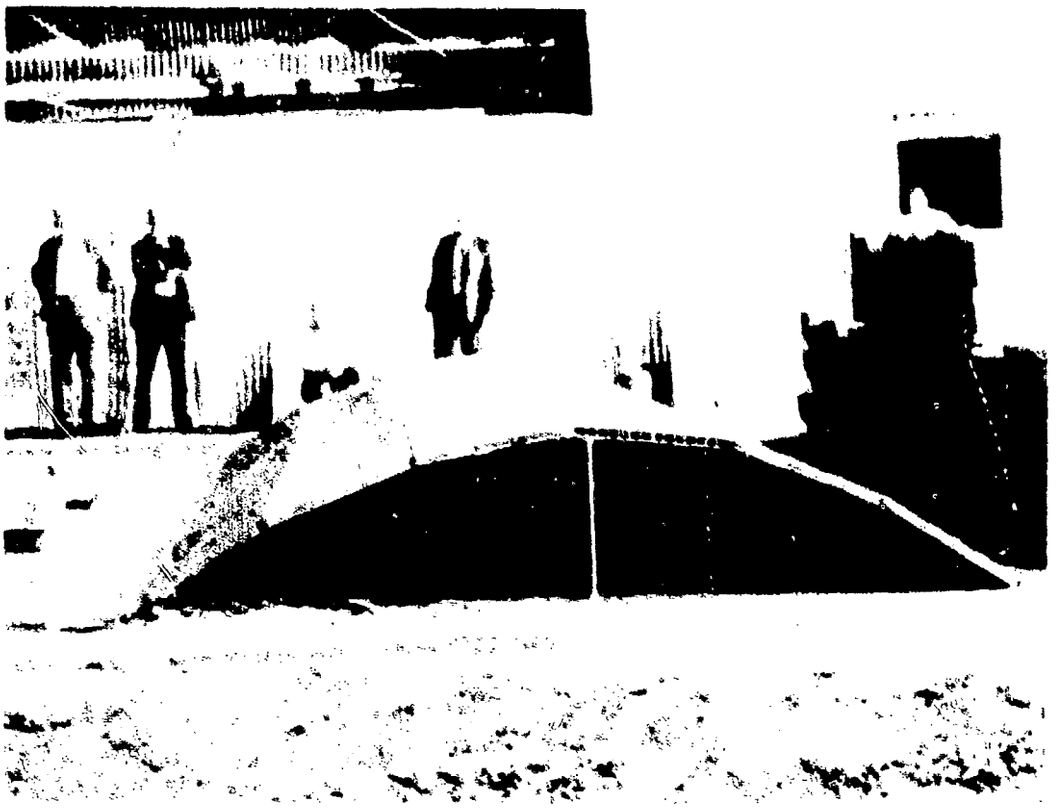

Figure A4 Print from film showing maximum buckling height (approximately 30 in.)

(assuming buckling has been induced by the movement of the aircraft) for the development of the bow wave, and the mat behind the bow wave would have to move a horizontal distance greater than 20 in. This horizontal force is the force which had to be applied to the runway in front of the aircraft and assumes that none was taken by tension in the runway behind the aircraft. A horizontal thrust of 80,000 lb would mean that the difference in the coefficient between the tire and mat and the coefficient between the mat and subgrade would be approximately 0.2. Although Test No. 5 (see Figure A13) indicated a coefficient difference of only 0.1, it is felt that a difference of 0.2 or greater could have existed in the field.

7. If the transverse joint of the AM2 mat remains connected, the joint is capable of carrying very large loads in tension. Test No. 4 (see Figure A12) indicated the strength of one panel to be in the order of 200,000 lb. The weight of the runway is approximately 600 lb/ft of runway and should be able to resist 300 lb of horizontal thrust (assuming a 0.5 coefficient of friction between the runway and membrane). If only 100 ft of runway behind the aircraft were effective, 30,000 lb would be required to slide the mat. Test No. 1 indicated mat movement behind the aircraft at greater distances. Thus one question is, why did the mat not take the horizontal thrust by tension in the mat behind the aircraft? The reason appears to be a combination of joint failures and the accumulation of joint slack. Although the transverse joint will take large tensile forces, the joint will become disconnected with small rotational movement of the mat, particularly if the C-rail is damaged. Several joints behind the aircraft were noted to be disconnected.

a. Four panels in buckling shape

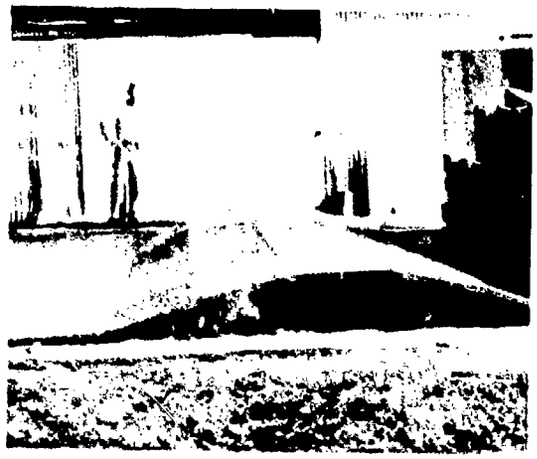

b. Fifth panel has popped up in buckling shape

c. Sixth panel popping up

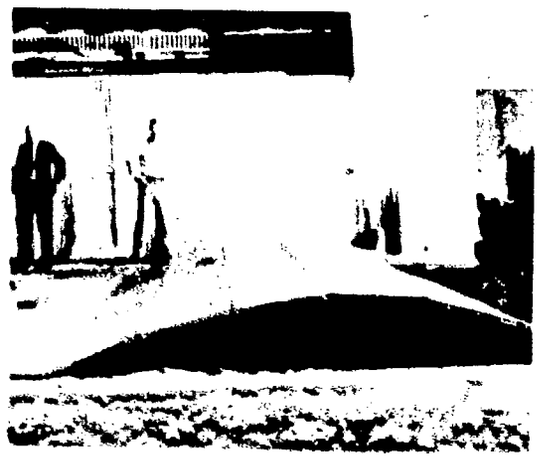

d. Mat in final buckling form

Figure A5. Series of prints from motion picture film showing change in buckling shape

8. After studying the available information, I have the following comments on the subject tests.

a. If only negligible tensile forces develop behind the aircraft, then the horizontal thrust produced by the aircraft braking is sufficient to cause buckling of the AM2 mat.

b. In the failure at Dyess AFB, buckling did occur and the mat failed by bending of the transverse joint.

c. The cause of failure lies in the basic design of the AM2 mat, although the worn condition of the mat at the time of the failure was a contributing cause. The worn condition is felt to be the primary reason for disconnections noted behind the aircraft.

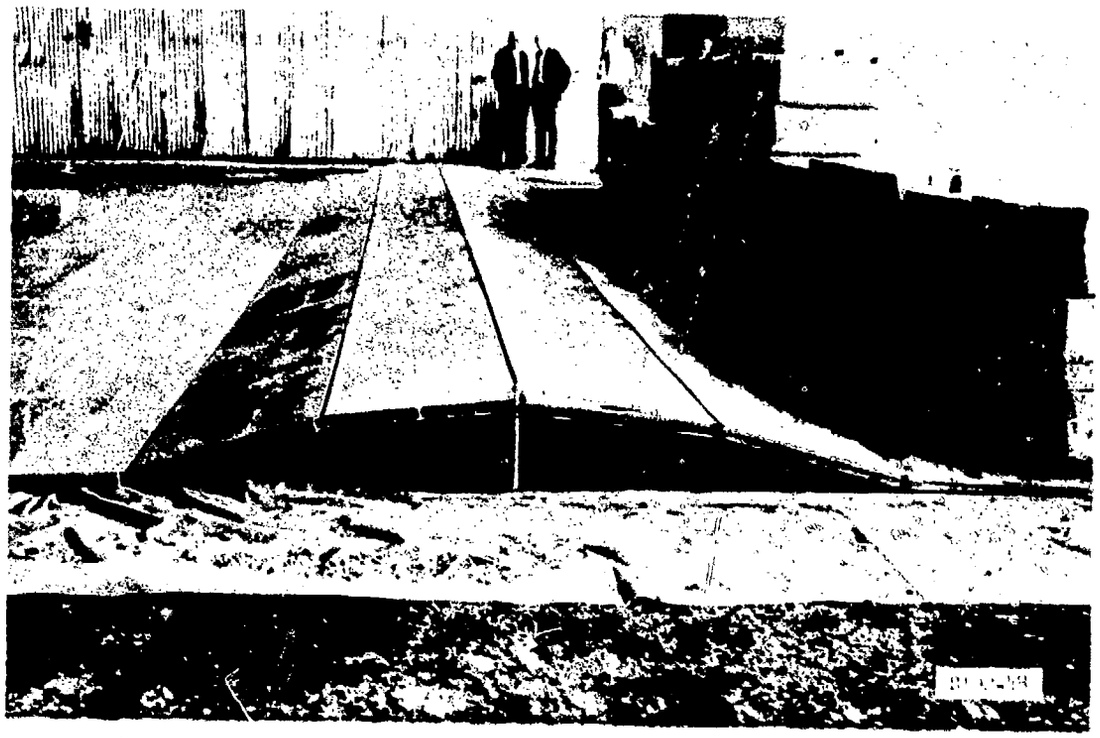

Figure A6. Mat with four panels buckled just prior to attainment of final buckling shape

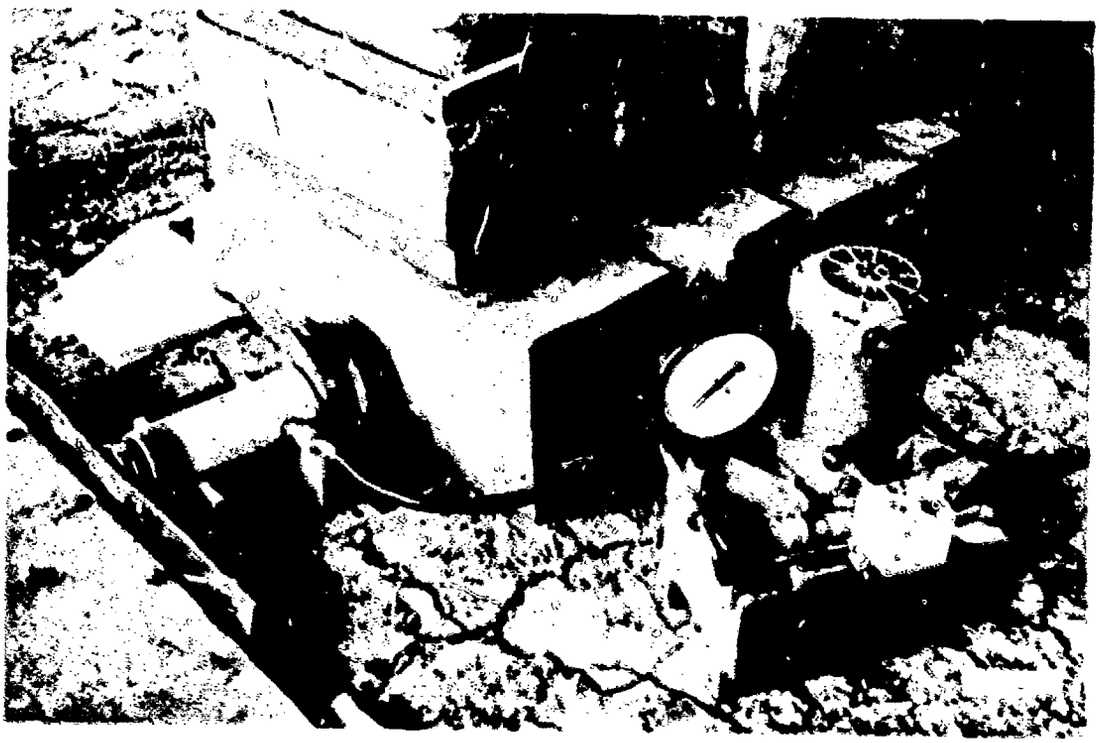

Figure A7. System for applying horizontal thrust to mat

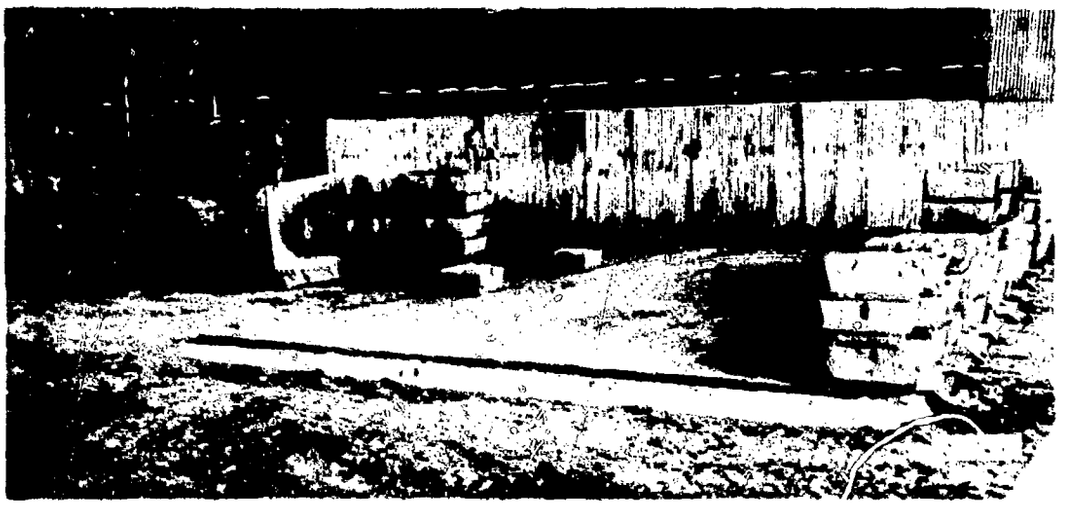

Figure A8. Overall view of mat section and anchorage system

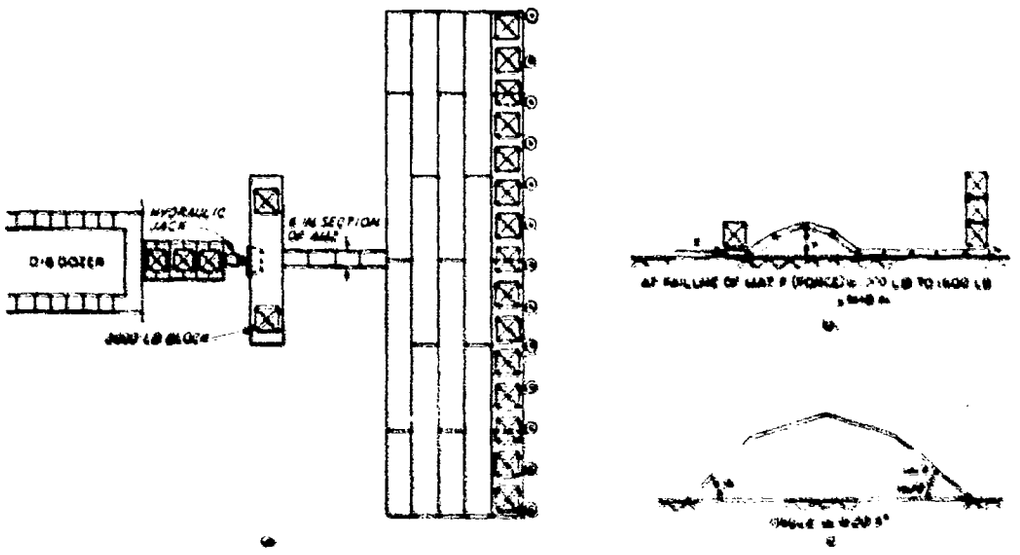

Figure A9. AM2 buckling Test No. 2 with typical sections of mat as buckled

d. The AM2 mat may be made more stable by either changing the geometric shape of the panel, changing the lay pattern, increasing the bending resistance of the longitudinal joints, decreasing the joint slack so that more horizontal thrust is taken by tension, increasing the resistance to transverse disconnection, or by increasing the coefficient of friction between the mat and subgrade.

9. In Test 1A, the mat first buckled at approximately 60,000 lb after buckling load dropped to about 30,000 lb. In Test 1B, the mat would not buckle at 75,000 lb, so buckling was induced. Four planks were in the first buckling mode. The final mode was as shown in Figure A7.

Figure A10. Cross section of mat showing mat failure from buckling

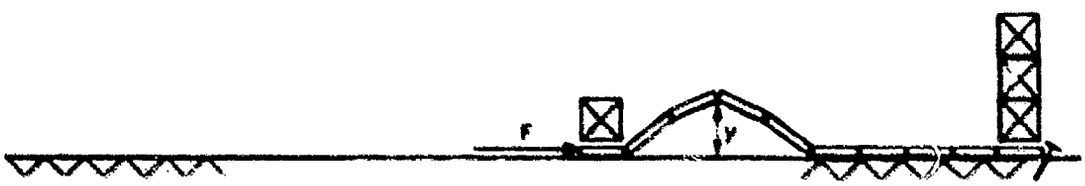

AT FAILURE OF MAT F = 10,000 LB
y = 20 IN.

Figure A11. AM2 buckling Test No. 3 with 6-ft panels in layout (basic layout same as Test No. 2 with 6-ft panels replacing 8-in panels)

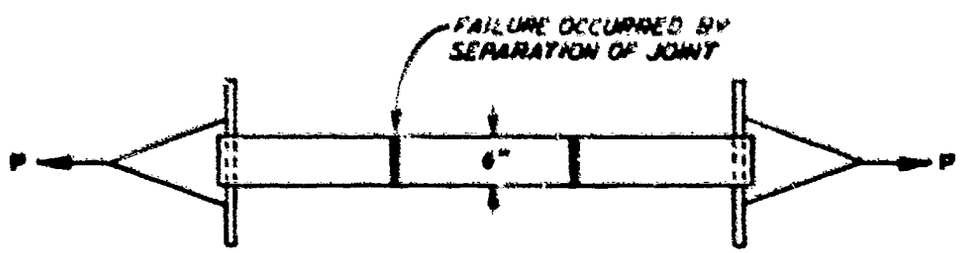

P (PULL, IN /LB) AT FAILURE = 8000 LB

Figure A12. AM2 Test No. 4 tension test with 6-in sections of mat

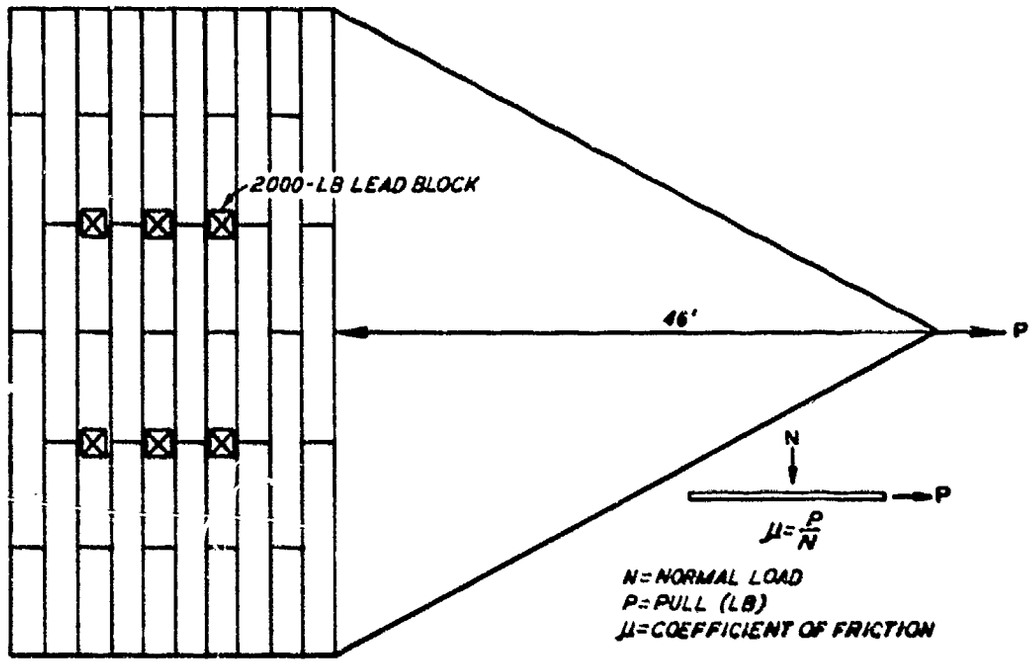

Figure A13. AM2 Test No. 5

Table A1
Coefficient of Friction for Two-Piece AM2 Mat
36 ft by 20 ft by 6.1 psf = 4392 lb

Run	Loading Condition	Time sec	Distance ft	N, lb	F, lb	μ
1	Mat only on membrane	8	6.0	4,392	2,200	0.50
2	Mat w weights on membrane	8	11.7	16,392	7,800	0.48
3	Mat only on subgrade	8	9.0	4,392	3,100	0.71
4	Mat w weights on subgrade	8	9.0	16,392	10,400	0.63

10. During Test No. 1, the load required to buckle the mat from a flat position varied, depending on how flat the mat was lying. Once buckling had been induced, 30,000 to 40,000 lb of force was required to form a wave six panels in length to a height of approximately 30 in. The force required to sustain buckling tended to increase slightly as the joint began to transfer movements.

11. Findings from Test No. 2 (buckling of 6-in. section of mat) are

a. The strength of the joint in bending is from 3000 to 4500 in.-lb per in. of mat, or from 36,000 to 54,000 ft-lb per 12-ft panel.

b. The failure of the male rail caused the joint failure. The first failure was in the top skin of the male rail; then the lower skin failed.

c. This mat failure was the same type of failure observed at Dyess AFB.

12. The findings from Test No. 3 (buckling of 6-ft mat) are:

a. The strength of the joint was 2800 in.-lb per in. or 33,000 ft-lb per 12-ft panel.

b. Failure of the top skin of the male rail caused joint failure.

c. The angle α was approximately 24.5 deg.

d. After buckling began, only about a 20 percent increase in force was required to fail the mat.

13. The findings from Test No. 4 (tension test) are:

a. The strength of an undamaged joint was approximately 1500 lb per in. of panel or approximately 216,000 lb per 12-ft panel.

b. The mat failed in tension by bending of the C-rail and the joint becoming uncoupled.

c. The upper part of the C-rail bent upward 0.1 in.

d. With the C-rail bent, the mat had to rotate only about 12 deg to become uncoupled. Normally, on undamaged mat, the rotation required for the mat to become uncoupled is about 30 deg.

14. The findings from Test No. 5 (determination of the coefficient of friction) are:

a. The coefficient of friction between the bottom of the mat and polyethylene was approximately 0.8.

b. The coefficient of friction between the bottom of the mat and subgrade was approximately 0.65.

c. Lower coefficient values were obtained with the loaded mat than were obtained when the mat was not loaded. The number of tests conducted were insufficient to establish a conclusive relationship between the normal load and the coefficient of friction.

15. The conclusions (Tests No. 1-5) related to failure are:

a. The major damage was caused by the formation of a bow wave in front of the main landing gear. The mat failed by bending the side joints.

b. The force required to form and maintain this wave would be at least 50,000 lb.

c. It is possible that joint separations behind the aircraft could have aided in the formation of the bow wave.

d. For the bow wave to form, considerable movement of the mat was required (2 to 3 in.).

e. For the development of a force sufficient to buckle the mat, the difference in the coefficient of friction between the mat and tire and between the mat and subgrade would have had to be at least 0.2. The test conducted indicated a difference of only 0.1. It is most likely that the test conditions for the determination of the coefficient of friction between the mat and membrane did not duplicate the field conditions.